Evidence of subduction, collision, and extension in northern Borneo: Constraints from receiver functions

Amy Gilligan(1),* David G. Cornwell(1), Nicholas Rawllinson(2), Felix Tongkul(3), Simone Pilia(4), Tim Greenfield(2), Conor A. Bacon(5)

1. *School of Geosciences, University of Aberdeen, Aberdeen, UK*
2. *Department of Earth Sciences, University of Cambridge, Cambridge, UK*
3. *Faculty of Science and Natural Resources, Universiti Malaysia Sabah, Kota Kinabalu, Malaysia*
4. *College of Petroleum Engineering and Geosciences, King Fahd University of Petroleum and Minerals, Dhahran, Saudi Arabia*
5. *Lamont-Doherty Earth Observatory, Columbia University, Palisades, New York, USA*

** Corresponding author: amy.gilligan@abdn.ac.uk*

Highlights

- A new Vs model for northern Borneo is obtained from P-receiver functions jointly inverted with a global surface wave model.
- Crustal thickness is found to vary from 24km beneath central northern Borneo, to 60km beneath the Crocker Range.
- We image Dangerous Grounds crustal material underthrust beneath western Sabah following subduction and collision.

Abstract

Northern Borneo (Sabah) has a complex geological history, experiencing multiple episodes of subduction, magmatism, uplift, subsidence, and extension since the Mesozoic. This includes the subduction of the proto-South China Sea beneath Sabah, terminating ~21 Ma; a postulated later phase of subduction of the Celebes Sea plate, terminating ~9 Ma; extension in central Sabah ~9-10Ma; rapid emplacement and exhumation of a granite intrusion ~7Ma, and the development of a fold-thrust belt offshore during the last 5 Myr. While these events have left imprints in the surface rock record, it has not been possible, until recently, to investigate deeper lithospheric processes that have shaped Sabah. The installation of 46 broadband seismometers - the northern Borneo Orogeny Seismic Survey (nBOSS) - between 2018 and 2020 means that it is now possible to constrain the architecture of the crust and uppermost mantle beneath Sabah. We use two years of passive seismic data recorded by the nBOSS network, and an additional 24 Malaysian Meteorological Service broadband seismometers in Sabah to calculate P-wave receiver functions. We then use these in a joint inversion with surface wave data to obtain shear velocity models of crustal structure. The thickest crust (60km) occurs beneath the Crocker Range, while the thinnest crust (24km) is found in central Sabah, potentially recording Miocene extension. The crust beneath the 4095m high Mt Kinabalu is also comparatively thin. Distinct, low-velocity, dipping anomalies identified in our shear wave velocity models provide clear evidence for underthrusting of Dangerous Grounds continental crust following subduction and collision.

Plain language summary

The processes that happen because of the movement of tectonic plates leave an imprint on the interior of the Earth, and to fully understand these processes we need to make images of the subsurface. Over the last 65 Million years, the northern part of the island of Borneo (Sabah) has been affected by multiple tectonic events including potentially two episodes of subduction – where one tectonic plate descends beneath the other - and mountain building due to the collision between the Dangerous Grounds and Sabah. Until recently there were insufficient instruments to make the measurements necessary to obtain images of the interior of the Earth beneath Sabah. In 2018 this situation was transformed with the installation of 46 seismometers – instruments that detect earthquakes. We use the records from distant earthquakes recorded by these and pre-existing seismometers to build up a picture of the Earth ~100km below the surface of Sabah. Our work reveals that the thickness of the crust beneath Sabah varies from 24km in central Sabah, to 60km beneath the Crocker Range. We also image part of the Dangerous Grounds crust now situated beneath Sabah, emplaced as a result of the collision between these two tectonic blocks.

Introduction

Subduction is fundamental to the growth of continents (e.g. Foley et al., 2002), driving plate motion (Forsyth and Uyeda, 1975), and long-term climate regulation (e.g. Johnston et al., 2011). Eventually subduction will come to an end (e.g., via continent-continent collision), and this may result in magmatism, exhumation, rapid uplift, and subsidence (e.g. Zandt et al., 2004, Levander et al., 2011, Li et al., 2016). The processes occurring in these post-subduction settings remain, at present, poorly understood. Given that subduction has been happening on Earth for at least 1.8 Ga (Weller and St Onge, 2017), explaining post-subduction processes is vital, not just for our understanding of present-day tectonics, but also for interpreting the deep geological record.

Northern Borneo is an ideal location for studying post-subduction processes. It is thought to be the site of two subduction systems that have terminated since the start of the Neogene: the subduction of the proto-South China Sea (pSCS) until ~21 Ma (Lai et al., 2021, Hall 2013, Morley and Back, 2008, Tongkul 1994, Tongkul 1991) along the present-day NW coast of Sabah, and the subduction of the Celebes Sea along the present-day SE coast of Sabah, which terminated ~9 Ma (Lai et al., 2021). In this study we use passive seismic data recorded by a network of broadband seismometers deployed across the Malaysian state of Sabah, situated on the northern end of the island of Borneo, between 2018-2020 (Figure 1) to image the crust and mantle lithosphere to both improve our understanding of the tectonic setting of northern Borneo and provide new insight into subduction termination and post-subduction processes.

Geology and tectonic setting of Sabah

The diverse surface geology of Sabah is testament to the rich range of tectonic processes that have affected the northern part of Borneo since the

Mesozoic. Some of the oldest dated rocks are those of the Segama Valley Felsic Intrusions (250 and 241 Ma) (Burton-Johnson et al., 2020) in eastern Sabah, which are intruded into ophiolitic rocks, with some subsequent, mineralogically distinct, felsic intrusions in the same area being dated at ~178 Ma. It has been proposed (Burton-Johnson et al. 2020, Balaguru and Nichols, 2004) that these formed in an extensional basin in a suprasubduction setting, which was then uplifted and eroded in the latest Cretaceous or earliest Paleocene, around 66 Ma (Balaguru and Nichols, 2004). A recent study by Tian et al., (2024) has dated, using Zircon U-Pb ages, ophiolites in Sabah to 248-244 Ma, which they argue formed in a small extensional setting related to the subduction of Paleo-Tethys and the start of subduction of the Paleo-Pacfiic plate.

By the Paleocene (66-56Ma) subduction of the proto-South China Sea towards the south-east beneath what is now the western edge of Sabah had begun (e.g., Hutchison et al., 2000, Rangin et al., 1999). Cumulate gabbros, part of the Sabah Ophiolite, in the Tongod-Telupid area have been dated to 42.65 ± 0.51 Ma (Lai et al., 2021), and from their geochemical signature are thought to have formed in a back-arc basin. Similarly, the geochemistry of the Sandakan andesitic tuff (33.9 ± 7.7 Ma, Bergman et al., 2000) could also suggest a back-arc basin setting (Lai et al., 2021, Hutchison et al., 2000). In the fore-arc, thick (~9000 m) sedimentary successions of deep marine sandstones, shales and minor conglomerates, are present in the NE-SW trending Crocker Basin (Balaguru and Nichols, 2004).

Opening of the South China Sea (~33-32 Ma, (Franke, 2013, Barckhausen et al., 2014, Li et al., 2014)), driven by subduction of the proto-South China Sea, pushed continental slivers, including the Dangerous Grounds and Reed Bank blocks, towards Borneo (e.g., Tongkul 1991, Tongkul 1994, Hutchison et al., 2000, Hall 2013, Rangin et al., 1999). Subduction of the proto-South China Sea continued in the earliest part of the Miocene (24-21 Ma, Lai et al., 2021 and references therein), however, at around 21 Ma the Dangerous Grounds block collided with and then underthrust northern Borneo (Lai et al., 2021, Hall 2013, Morley and Back, 2008, Tongkul 1994, Tongkul 1991), which ultimately caused subduction to cease. This collision led to uplift above sea level (Burton-Johnson et al, 2020, Hall 2013, Morley and Back, 2008). However, by the end of the Early Miocene, most of Sabah was at or below sea level once more, with low hills where the Crocker Range is today (Hall 2013, Cottam et al, 2013).

Subduction of the Celebes Sea beneath eastern Sabah began at a similar time to the termination of subduction of the proto-South China Sea and may have been a result of changes in regional stresses due to the Sabah-Dangerous Grounds collision (Lai et al., 2021, Linang et al., 2022). In the Dent Peninsular, rocks that are the product of arc magmatism have been dated to 18.8-17.8 Ma and in the Semporna Peninsula to 18.2-14.4 Ma (Macpherson et al., 2010). It is, however, important to note that the idea that there was northwards subduction of the Celebes Sea is contested (Burton-Johnson and Cullen, 2023). A slab from this subduction event has yet to be imaged in the mantle.

Roll-back of the Celebes Sea subduction from 19 Ma led to extension in the Sulu Sea and in Sabah (Hall, 2013). Thick (~6 km) successions of carbonates, shallow marine, and fluvio-deltaic sediments, including coals, were deposited in a basin in Central Sabah (Tongkul and Chang, 2003, Balaguru and Nichols 2004, Burton-Johnson et al., 2021). The coastal/shelf environments for all these sediments, including coal that was buried to 3 km depth (Baluguru and Nichols, 2004), means that subsidence must have continued over a prolonged period. Tsikouras et al., (2021) argue that the major increase in extension suggested by Huang (1991) between 9 and 11 Ma led to rifting in Ranau area, and suggest that sea-floor spreading took place in the Telupid area. This is disputed by Cullen and Burton-Johnson (2021) who argue that while extension took place, the Sulu Sea rift did not extend into Sabah. In a recent review Lai et al., (2021) suggest that Celebes Sea subduction beneath Borneo terminated ~9 Ma.

The Kinabalu pluton, which forms the 4095 m high Mt Kinabalu, was intruded into peridotites and the Crocker formation between 7.85 and 7.22 Ma, at a depth of 3-8 km (Cottam et al., 2013). Between 6.6 and 5.8 Ma it was rapidly cooled and exhumed with rates of up to 7 mm/yr (Cottam et al., 2013). The emplacement and exhumation of the Kinabalu pluton likely occurred in an extensional setting (Hall et al., 2013, Burton-Johnson et al., 2019).

Sabah only became fully emergent above sea level by the end of the Miocene to early Pliocene (~5 Ma), and uplift has occurred since (Roberts et al., 2018, Hall 2013, Morley and Black 2008). This includes uplift of the circular basins, such as the Maliau Basin, in central Sabah (Tongkul and Chang, 2003). During the Pliocene large-scale gravitational collapse occurred, seen in mass transport slumps, megaslides and extensional faults (Cottam et al., 2013), and as result of this, a fold and thrust belt has developed offshore of western Sabah (e.g., Spain et al., 2013, Franke et al., 2008, King et al., 2010). Around 5 Ma a change in the composition of volcanic rocks in eastern Sabah also occurs from calc-alkaline to a similar composition to ocean island basalts (OIB), (Macpherson et al., 2010). Volcanism in eastern Sabah has continued into the Holocene, potentially as recently as 24-27 ka based on radiocarbon dating of carbonised material (Kirk, 1968; Bellwood, 1988; cited in Tjia et al., 1992), although Takashima et al., (2004) date the youngest volcanics in their study using thermo-luminescence to 90 ka.

Previous geophysical work

Regional-scale tomographic studies of South-East Asia have observed anomalously high seismic velocities in the upper mantle beneath Sabah at depths of ~100-300 km (e.g., Amaru, 2007, Tang and Zheng, 2013, Hall and Spakman, 2015, Zenonos et al., 2019, Wehner et al., 2022). These high velocities are attributed to the presence of slab remnants in the upper mantle. While the earlier body-wave studies (e.g., Amaru, 2007, Hall and Spakman 2015, Zenonos et al., 2019) had limited resolution beneath Sabah, thus bringing the existence of higher velocities into question, the full-waveform model of Wehner et al., (2022), SASSY21, uses data from the same dense seismic network in Borneo used in this study, and so has improved resolution in this region. Other results from this dense seismic network – the nBOSS network – are described below.

In a Sabah-focused P- and S-wave tomographic study, also using nBOSS data, Pilia et al., (2023a), observe two distinct fast velocity anomalies in the upper mantle beneath Sabah. One, an elongate anomaly at depths >250 km underlying most of the Crocker Range, is attributed to the proto-South China Sea Slab, while the other, a relatively narrow (<100 km) anomaly between ~150 and 300 km depth in central Sabah, is interpreted to be a lithospheric drip from the volcanic arc root beneath the Semporna Peninsular. Pilia et al., (2023b) perform thermo-mechanical modelling and suggest that the downwelling drip can cause extension and crustal thinning, resulting in melting and exhumation of sub continental material. As such, the 'Semporna drip' may play an important role in the emplacement of the Kinabalu pluton, as well as explaining subsidence and uplift, and the lavas with an OIB composition in eastern Sabah.

Bacon et al., (2022) investigate anisotropy beneath Sabah using XKS splitting measurements extracted from nBOSS teleseismic data. Their results demonstrate that fossil anisotropy in the lithosphere is the main control on anisotropic properties in this post-subduction setting. They observe fast directions parallel to the strike of the Crocker range in western Sabah, likely imparted when the Dangerous Grounds block collided with Sabah. In the east of Sabah, fast directions are sub-parallel to the direction of spreading in the

Sulu Sea, suggesting that the anisotropic fabric may have developed as a result of extension, while the null results they observe in the southeast may arise due to the lithospheric drip observed by Pilia et al., (2023a).

Roberts et al., (2018) suggest that removal of the lithosphere and replacement by hot asthenospheric material could explain the relatively rapid uplift and erosion rates observed in Sabah (~0.1-0.3 mm/yr, Morely and Back, 2008). They base their estimates of thin lithosphere on regionally extensive slow shear wave velocities at 100-200 km depth in the global tomographic model of Schaeffer and Lebedev (2014). However, in recent 2-plane-wave tomography of Sabah from Greenfield et al., (2022), average lithosphere thickness beneath Sabah is found to be ~100 km, with the lithosphere only being thin (<50km) beneath the Semporna Peninsula, consistent with the work of Pilia et al., (2023b) that suggests that the lithosphere here has dripped off.

Until recently, estimates of crustal thickness in Sabah had been limited. Holt (1998) modelled gravity data from Sabah and suggested that the whole of Sabah was underlain by crust >30 km thick, that crustal thicknesses beneath the Crocker Range were ~50 km, and 39 km beneath central Sabah. Estimates of 27±3 km and 33±2 km beneath seismometers KKM and LDM near Kota Kinabalu and Lahad Datu respectively have been made by Lipke (2008) from H-κ stacking of receiver functions, while Syuhada et al., (2022) invert receiver functions from KKM and LDM using the Neighbourhood algorithm and find crustal thicknesses of 30 km and 26 km, respectively. Latiff and Othman (2020) invert receiver functions from KKM and find a crustal thickness of 40km. A regional crustal thickness map derived from surface wave data made by Tang and Zheng (2013) estimates crustal thickness beneath Sabah to be 27.5-32.5 km. The deployment of the nBOSS seismic network between 2018-2020 has allowed for more detailed studies of crustal thickness across the whole of Sabah to be conducted. Greenfield et al. (2022) use the 4.1 km/s velocity contour in their shear wave velocity model as a proxy for the Moho and suggest that crustal thicknesses vary from 25-55 km, with the thickest crust beneath the Crocker Range and the Dent Peninsula, and the thinnest crust in north east Sabah. Linang et al. (2022) use Virtual Deep Seismic Sounding (VDSS) to estimate crustal thickness in the range 21 - 46 km, with a similar pattern of thicker and thinner crust.

Until now, due to a lack of seismic instrumentation in the region, it has not been possible to derive a detailed model of the seismic velocity structure of Sabah's crust. Consequently, debates have continued to emerge (e.g., Milsom et al. 2001, Cullen and Burton-Johnson, 2021) about the nature of the crust beneath this part of Borneo and the processes that have shaped it. Fone et al., (2024) use data from the nBOSS network to develop an ambient noise phase velocity model of the crust to 36s period, and invert their surface wave data for a shear velocity model. This model is able to well resolve lateral features greater than 50km well, highlighting the heterogenous nature of the crust in Sabah, but is limited in its resolution of vertical contrasts.

In order to further understanding of crustal and upper mantle structure, particularly vertical discontinuities, we calculate radial P-wave receiver functions at 70 seismic stations, including the recent nBOSS deployment across Sabah, and jointly invert these with surface wave data to develop a detailed shear velocity model of the crust in Sabah, allowing us to map the Moho geometry beneath. These results provide important constraints on processes that have shaped the region.

Data and Methods

Broadband teleseismic data in this study come from two seismic networks deployed in Sabah (Figure 1, Supplementary Table 1). The temporary nBOSS network of 46 seismometers, installed mostly on a ~40x40 km grid , with a mean interstation distance of 37.5km (Bacon, 2021), between March 2018 and January 2020, consisted of 18 Güralp 3ESPD instruments and 28 Güralp 6TD instruments (Rawlinson, 2018, Pilia et al., 2019). We also used data from the Malaysian Metrological Service permanent seismic network. In Sabah, this consists of 24 permanently installed Streckeisen STS2/2.5 and SS1-Ranger seismometers, predominantly located in regions of elevated seismicity around Mt Kinabalu and Darvel Bay.

Calculation of radial P receiver functions from 3-component seismograms of teleseismic (30-90° epicentral distance) earthquakes allows us to investigate the structure of the crust, including determining Moho depth and identifying layering within the crust.

We performed the initial quality control of the seismograms in two stages. First, a total of 27,660 3-component seismograms from March 2018-

September 2018 for earthquakes M_w >5 that met the distance criteria were visually inspected. Where the P-wave signal-to-noise ratio was high (e.g., a P arrival could clearly be identified) on all 3 components, these seismograms were classified as ‘good’ and were taken forward for further analysis. All other seismograms were rejected and classified as ‘bad’. Using this classified data set we developed a deep learning algorithm to determine the probability of a 3-component seismogram being suitable for further analysis. The annotated (good or bad) seismograms were converted into spectrograms and 80% of the data were used to train an image classification convolutional neural network, ResNet50, pretrained on ImageNet (He et al., 2016). The data classification algorithm was then tested using the remaining 20 per cent of the data and had a 92.7 per cent accuracy. A total of 57,858 3-component seismograms from September 2018-January 2020 were then used with the classification algorithm, and only those classified with a greater than 50 per cent probability of being ‘good’ were visually inspected. This significantly reduced the time needed for this stage of data quality control, while resulting in a similar proportion of events being taken forward for further analysis.

After initial quality control, 14,447 seismograms were used to calculate receiver functions using the time-domain iterative deconvolution method of Ligorría and Ammon (1999), with a gaussian width of 1.6, corresponding to a frequency of 0.9Hz. A guassian width of 1.6 provides a good balance of resolving detail in the crust, while avoiding the risk of overinterpreting noise. Further quality control steps included removal of receiver functions with a poor fit (<70 per cent), and those which appeared noisy, oscillatory or anomalous to other receiver functions from a similar distance and backazimuth on visual inspection. This left a remaining dataset of 3338 receiver functions. Eight stations, one from the nBOSS network, and seven from the Malaysian Metrological Service permanent seismic network, had no usable receiver functions. For stations with usable receiver functions, the number of receiver functions at individual seismometers ranges from 9 at SPM to 183 at SBA8 (Supplementary Table 1, Supplementary Figure 1). This is due to variations in the amount of data available from individual stations and the noise levels at the installation sites.

Receiver functions at an individual station are stacked together to reduce noise, and these stacks are used in an inversion for crustal velocity structure. While useful, the interpretation of receiver functions on their own is inherently non-unique (Ammon et al., 1990). Therefore, to ensure that shear velocities we obtain from inversions of receiver functions are realistic for this region, we jointly invert the receiver functions with fundamental mode Rayleigh wave group velocity dispersion curves extracted from the GDM52 global compilation (Ekström, 2011) for each station location for a period range 25–250 s. This model is relatively coarse ($1^{\circ} \times 1^{\circ}$), does not see much variation in group velocities beneath Sabah (Supplementary Figure 2), and with a minimum period of 25s, is most sensitive to depths of 25km and below, corresponding to the mid to lower crust and upper mantle in this area. We are primarily concerned in this study that the inversions result in velocity models that fit the receiver function data.

The radial P receiver function stacks, together with the dispersion curves, for each station were inverted for shear velocity structure using joint96 (Herrmann, 2013), an iterative linearised least squares inversion method. Several starting models were tested including constant values of 4.48 km/s, (mantle velocity in the ak135 model - see Kennett et al., 1995), 4.28 km/s, and 3.70 km/s and a Vp/Vs value of 1.74 down to 100 km depth, parameterised into 2 km thick layers, overlying ak135 (Supplementary Figure 3). While there are some small variations in the absolute shear velocities due to differences in the starting models, they are sufficiently small to not alter the interpretation of the structure. We test different relative weights (p value in joint96) of surface waves to receiver function data in the inversion: 0.5, 0.1, 0.05 and 0.01. Models with p=0.5 are smoother than those with a lower p value, reflecting the greater contribution of surface wave data. Overall, the models show little variation in structure with p value, indicating that the recovered features are robust (Supplementary Figure 4).

In order to test the stability of the results, the receiver functions at each station were divided into 3 time periods (March 2018-Sept 2018, Sept 2018-March 2019, March 2019-Jan 2020) and were stacked and inverted separately. There was very little difference between the resulting models and those obtained from the complete dataset (Supplementary Figure 5). This can be considered a form of bootstrapping, and gives us further confidence that the results are robust

Results

Individual receiver functions

Plotting individual receiver functions with respect to backazimuth (e.g Supplementary Figure 1, Supplementary Figure 6), shows that for some stations there is a degree of variability for events at different backazimuths. There are a number of potential causes of this, including short-length scale variation in crustal structure, anisotropy in the crust, and dipping layers in the crust. Unfortunately the backazimuthal range of events in this study is limited, with events being mainly to the north east or south east of the seismometers, meaning it is not possible to model the cause of the backazimuthal variation effectively. Because of this limitation, we consider all receiver functions at a station in a signal stack.

At some stations we observe receiver functions that do not fit with the typical idea of a receiver function, which in some automated QC approaches would have been rejected. One of the most extreme examples of this are the receiver functions computed for events recorded by the station SBG3 (Supplementary Figure 6). Here, the amplitude of the first arrival is relatively low, merging with a large amplitude positive arrival at ~2. There is a large amplitude negative arrival at ~4s, and a large amplitude positive arrival at ~5s. At this station there are 52 individual receiver functions that have this pattern (i.e all those with north easterly or south easterly backazimuths). Further, the Malaysian Metrological Service seismometer PTM, located ~20km from SBG3, also shows similar pattern of positive and negative arrivals. PTM is a different type of seismometer, deployed in a different way to SBG3. The consistency between multiple events, and similarities between receiver functions at different, but relatively close, locations suggests that, while these receiver functions are not necessarily typical, they do reflect real crustal structure.

Stacked receiver functions

Stacked receiver functions at each station are plotted on cross-sections across Sabah (Figure 2). Cross-section A (Figure 2 (a)) cuts through the highest topography in Sabah in the region around Mt Kinabalu. Heading SE from the NW coast there is a positive arrival that decreases from ~4.5 s to ~3 s delay time at the stations immediately beneath the highest topography. Moving further SE, the delay time of this prominent positive arrival then increases to ~7 s at station SBE4 (dark grey dashed line). At stations to the SE of Mt Kinabalu, this positive arrival is preceded by a large amplitude negative arrival that similarly shows an increase in arrival time from ~3 s at SBF2 to ~5 s at SBE4 (light grey dashed line). There is a clear change in the character of the receiver functions from ~200 km along the cross section, with the portion of cross-section A between SBD5 and SBD7 having a large amplitude positive arrival at ~6-6.5 s (dark grey dashed line).

In cross-section B (Figure 2 (b)), the stations in the Crocker Range have a relatively consistent large amplitude positive arrival (dark grey dashed line) at ~4 s, while at SBB3 and SBD4, immediately to the SE, the largest amplitude positive arrival appears to be at ~6.5 s. Between these stations and those in the vicinity of the Maliau Basin there is a strong positive arrival at ~3.5 s, while at the stations near to the Maliau Basin there is an arrival at ~5 s. At the south-east end of the cross-section, in the Semporna Peninsula, the largest positive arrivals, after the direct P arrival, is again at a shorter delay time of around 4 s.

The peak at ~0 s should correspond to the direct P arrival; however if there are low-velocity sediments in the uppermost crust the P-to-S conversion from the base of these may interfere with the direct P resulting in the first positive arrival being shifted away from 0 s. This is observed at several sites, e.g., SBD6 (Figure 2 (a)) and MALB (Figure 2 (b)) and is anticipated given the thick sedimentary basins (>6 km sediments, Hall, 2013) in Sabah.

Shear velocity structure

Using the 1-D shear wave velocity model beneath each station, 2D, composite velocity cross sections have been constructed using bicubic interpolation for several lines across Sabah, taking the velocity models for stations within 50km of the line. The models shown in Figure 3 are derived from the inversions that used p=0.1 and the 3.7 km/s starting model; however, the features remain consistent with the various weightings and starting models tested. Given the high weight of the receiver functions in the models shown, the descriptions and interpretations of the models are primarily concerned with changes in velocity, and relative velocities, rather than absolute velocities. The orientations of cross-sections A and B are chosen to be approximately perpendicular to the strike of the Crocker range, while cross-sections C, D, and E are chosen to help further elucidate the 3D crustal structure.

In cross-section A (Figure 3(a)), low velocity sedimentary basins, labelled as 1 in the cross-section, are illuminated offshore to the NW (SBG1) and in the south-eastern half of the cross-section (SE of SBE4), confirming the observation of a broadened, delayed P arrival in the receiver function stacks. Low velocities extend to depths of ~10 km. The most striking feature of this cross-section is a dipping high velocity layer, labelled 2, extending from SBE3 to SBE5 from ~5 km to 50 km depth, with a dip in the cross section to the SE, which overlies a low velocity layer, labelled 3, with a similar dip. This fits the pattern of arrivals seen in the receiver function cross-sections: a seemingly dipping transition from a high velocity to a low velocity layer resulting in a negative arrival, followed by a low to high velocity discontinuity with increasing depth.

In cross-section B (Figure 3(b)) low velocities, labelled 4, are also observed to ~10 km depth in the vicinity of known sedimentary basins between SBC4 and SBA7. The transition to mantle velocities (~ >4.2 km/s in this model) occurs at ~30-35 km depth in the north-western part of the cross section but deepens to greater than 40 km beneath SBC4. It shallows to ~25 km beneath SBB4 and SBC5, before deepening to ~35 km again beneath the Maliau Basin. This agrees with the pattern of positive arrivals observed in the stacked receiver functions, with those for stations between the Crocker Range and the Maliau Basin experiencing the shortest delay times. At the southeast end of cross-section B, the crust beneath SBA8 and SBA9 has lower velocities (~3.9 km/s in this model) at the gradient interpreted to be the Moho, labelled 5, than beneath stations elsewhere in the section.

The differences in crustal structure from south to north through western Sabah is highlighted in cross-section C (Figure 3(c)). The crustal structure at the north-east end of this section, to the north of Mt Kinabalu, has a different character to that in the central portion of the section (between SBD2 and SBE3). In the north east, very high velocities (>4.2 km/s in this model), labelled 6, are observed at ~20 km, while in the central portion they are generally low (<3.4 km/s in this model) at this depth in a somewhat discontinuous layer, labelled 7, likely the dipping low velocity layer observed in cross-section A. Cross-section D (Figure 3(d)) cuts to the east of the Crocker Range, through the Maliau Basin. In the south west of this section there is a northeasterly dipping transition from crust to mantle velocities (~4.2 km/s in this model) from 25 to 45 km depth between SBA3 and the Maliau Basin. At SBC5 it decreases sharply to a depth of 25 km, the depth it is also observed to be at between SBE4 and SBF4. Beneath SBD4 relatively high velocities are observed in the upper crust, labelled 8, and low velocities are observed between 25 and 45km depth. This location corresponds with where ophiolitic material is found on the surface around Telupid (e.g. Hall 2013) . In the south of cross-section E (Figure 3(e)), which cuts through the Semporna and Dent Peninsulas, the transition between crustal and mantle velocities at ~35 km depth is relatively gradual. This contrasts with further north, where this transition is sharper, and upper mantle velocities are faster.

Moho depth

The depth of the Moho beneath each station is picked from its corresponding 1-D shear velocity model at the depth that corresponds to the base of the steepest positive velocity gradient where shear velocity exceeds 4 km/s (Figure 4). The depth of the Moho is found to vary from 24 km at SBC6 and SBF4 to 60 km at MTM, although most other measurements are <48 km. The deepest Moho is found in a SW-NE trending band on the eastern edge of the Crocker Range, where the Moho depth exceeds 40 km. It is also relatively deep (40-44 km) beneath the Maliau Basin and beneath other circular basins to the north of the Maliau Basin, and to the west of the Segama ophiolite. The shallowest Moho depth (24-26 km) is found in a band between the Crocker Range and the circular basins, with changes in Moho depth of ~15-25 km occurring over short lateral distances (~20 km).

At the stations marked with white hexagons in Figure 4, it was not clear where the Moho should be picked. For instance, at a subset of stations (e.g., SBD6, SBD7, and SBC8) there is a very gradual increase in velocities over a wide (~40 km) depth range (Supplementary Figure 7), while at other stations (e.g., SBD5, SBE4, and SBG3) the models have two steep velocity gradients, both of which could represent plausible Moho locations given those found elsewhere in Sabah, for example at 28km and 58km for SBD5.

Discussion

Limitations of the models

The 1D velocity models obtained in the study have a number of limitations, which should be acknowledged in order to avoid over interpretation of the results. The receiver functions used in the inversions are single stacks for each station. This is done to reduce noise and source effects, however it may mask real complexity in crustal structure such as short-length scale lateral variations, anisotropy and dipping layers, which we have not be able to model due to the limitations imposed by the backazimuthal range of the events. Therefore it is likely that crustal structure beneath Sabah is more complex than shown in the models here.

In the inversions we use the relatively coarse, global model, GDM52 (Ekstrom, 2011), to help ensure the shear velocities are reasonable for the regional context. While the fits to the dispersion curves are reasonably good (Supplementary Figure 4), the focus of this study is the constraints provided by the radial P wave receiver functions, and so we prioritise the fit to the receiver functions for the models that we interpret. As the models are strongly weighted to the receiver functions, this means that the best constrained features in the crustal structure will be the velocity discontinuities, such as the Moho, rather than absolute velocities. In not using the dispersion measurements from Fone et al., (2024) and Greenfield et al., (2022), we are able to obtain an independent image of crustal structure, and thus make comparisons between the models, giving insight into the robustness of individual features and their potential interpretations.

Processes affecting crustal thickness

It is important to account for the effect of the interference between conversions and multiples (e.g., Gilligan et al., 2014): a consequence is that the largest signal on a receiver function should not necessarily be interpreted as being due to the velocity increase at the Moho. However, there is a consistent pattern between the positive arrivals observed in the stacked receiver functions and the velocity changes at the Moho observed in the models from joint inversion, suggesting that the receiver functions can, in this instance, provide an interpretable picture for trends in Moho depth.

The variations in crustal thickness across Sabah observed in this study are in general agreement with the estimates made by recent studies using 2-plane-wave tomography (Greenfield et al., 2022) and virtual deep seismic sounding (Linang et al., 2022): central Sabah appears to have significantly thinner crust than that beneath the Crocker Range and the Circular Basins (Supplementary Figure 8). One notable difference with the Greenfield et al., (2022) Moho estimate is beneath the Semporna Peninsular they observe thick crust (>55km), while in this study we observe crustal thickness of ~34km. This difference is likely to arise due to Greenfield et al., (2022) using the 4.1km/s shear velocity contour as a proxy for Moho depth, and this, as discussed below, may not be an appropriate velocity proxy for the lower crust/upper mantle beneath the Semporna Peninsular.

The pattern of thicker and thinner crust broadly agrees with the estimates of Holt (1998) using gravity data; however, between the Crocker Range and thickened crust beneath the circular basins we observe a significantly thinner crust (e.g., 25 and 24 km at SBC5 and SBC6 respectively) than the 32 km suggested by Holt (1998). Modelling gravity data is notoriously non-unique, and Holt (1998) uses a very simple model for crustal densities. Given the lack of other constraints on the properties of the crust at the time this may have been appropriate; however, the lateral and vertical heterogeneity of the crust demonstrated in this study indicates a more complex model is required, which may alter the estimates of crustal thickness from the gravity data.

It should be noted that the crust in this study is thicker throughout much of Sabah than was shown in interpretative cross-section of Hall (2013), which bases Moho depth off the results of Holt (1998), modified for denser material. Hall (2013)'s cross-section shows a maximum Moho depth of 40 km beneath the Crocker Range, and around 20 km beneath both the circular basins and the Dent and Semporna peninsulas. Further, our estimates of crustal thickness shows a significantly different pattern and depths to the estimates made by Tang and Zheng (2013). They report crustal thicknesses of ~27.5 to 32.5 km, increasing southward across Sabah, based on the depth of the 4 km/s velocity contour in their shear velocity model. This model encompasses the whole of the South China Sea and surrounding region and, as such, has more limited resolution in Sabah compared to this study and others (Greenfield et al., 2022, Linang et al., 2022) that have used the data from the nBOSS network. The thicker crust we observe, compared to earlier estimates, may mean that there is a larger contribution from regional tectonic shortening to the regional uplift observed by Roberts et al., (2018).

The relatively thick crust (>40 km) beneath the Crocker Range, particularly on the eastern side, is likely to have been thickened during the Sabah Orogeny (~23 Ma), when the Dangerous Grounds block collided with the western edge of northern Borneo at the final stage of the subduction of the proto-South China Sea (e.g., Hutchison et al., 2000, Hall 2013, Rangin et al., 1999). The velocity discontinuity picked as the Moho for many stations in the Crocker Range is the base of the SE dipping slow velocities seen in cross-section A, which we interpret as the base of the underthrust Dangerous Grounds crust.

Extension, related to the roll-back of the Celebes Sea slab (e.g., Hall, 2013), could have thinned the crust in central Sabah to 20-25 km. Indeed, Tsikouras et al. (2021) argue that the basalts they date to 9-10 Ma in the Telupid area, are rift-related, thus implying significant extension and crustal thinning, although this is disputed by Cullen and Burton-Johnson (2021). A double discontinuity is observed in our study in the 1-D velocity models at some stations (e.g., SBE4), and could indicate that it may not necessarily be appropriate to simply interpret the velocity gradient at ~20-25 km as a single Moho. If the crust is 20-25 km thick, the question as to the extent to which this crust may have been thinned remains, i.e., what was the pre-extensional crustal thickness? Greenfield et al. (2022) assume that it was 40-50 km, as is observed beneath the Crocker Range and circular basins, and thus calculate a stretching factor of 1.3-2. However, if this area was not significantly thickened during the Sabah Orogeny, which is plausible given the lack of underthrust Dangerous Grounds material observed in this study, then pre-extensional thickness may have been less to begin with.

Related to the question of pre-extensional thickness is whether the ~45 km thick crust observed beneath the Maliau Basin and other circular basins is a result of thickening during the Sabah orogeny (~23 Ma). After thickening it may have been separated from other thickened crust beneath the Crocker Range as a result of extension (e.g., in a crustal scale boudinage process as suggested by Linang et al. (2022)). Alternatively, the crust may have been thickened at a later point in time. Tongkul and Chang (2003) suggest that eastern Sabah experienced N-S compression in the mid Middle Miocene (~13 Ma), which led to the segmentation of the large basin in eastern Sabah that had been active in the Early Miocene, and NW-SE compression in the late Upper Miocene (~7-5 Ma), which enhanced the circular shape of the basins, with a period of sediment deposition in between these two compressional events. It may be that during these compressional episodes, potentially associated with Celebes Sea subduction, some crustal thickening occurred beneath the circular basins. More recently, Meju et al., (2024), using results from a magnetotelluric study, argue for thick-skinned deformation and deep crustal flow being involved with the evolution of Neogene ‘mini-basins’ offshore, which may be directly related to the onshore circular basins such as the Maliau Basin.

While areas of the highest topography may be anticipated to have some of the thickest crust, intriguingly beneath the stations in the vicinity of the 4095m high Mt Kinabalu the crust is only 30-35km thick. The Kinabalu Granite was emplaced between 7.2-7.8Ma (Cottam et al., 2013), well after the termination proto-South China Sea subduction, thus it would be expected that the crust in this region would have been thickened as a result of this collision. The thermomechanical modelling of Pilia et al., (2023b) shows that as a result of a downwelling drip, e.g the Semporna drip, a region of initially thick crust can be thinned. This thinning could facilitate melting of the lower crust, thus it may be that both the presence of the Kinabalu pluton and the thinner-than-anticipated crust we observe can both be explained by part of the lithosphere having dripped off beneath the Semporna peninsula.

Crustal structure

Given the diversity of the surface geology in Sabah, it is unsurprising that the crust shows considerable variation. The key elements of our interpretation are shown in Figure 5.

With the caveat that we have projected 1D velocity models from 50km around the lines of section, and thus may be masking some of the lateral variation perpendicular to this line, we interpret the low velocity (<3.4 km/s in our model) layer seen dipping to the south east from the west coast of Sabah to the eastern edge of the Crocker Range in Cross-section A (Figure 3(a)) as Dangerous Grounds material that has been underthrust beneath Sabah. Underthrusting of attenuated Dangerous Grounds crust has been proposed as the mechanism by which subduction of the proto-SCS stopped (e.g., Hall, 2013, Morley and Back, 2008, Hutchison, 2000). Fone et al., (2024) also observe low shear velocities at ~30km depth along a similar line of section, but this is arguably the first time it has been imaged as a dipping structure. Cross-section B (Figure 3(b)), which cuts to the south of Cross-section A, also has a low velocity layer at depths of 20-25 km. In this instance this layer does not seem to dip. We consider this to also be underthrust Dangerous Grounds crust, although this suggests potential along strike variation in the nature of the collision between Sabah and the Dangerous Grounds. Rangin et al. (1999), considering the whole of the proto-SCS, argue that the proto-SCS basin was narrower off the coast of Borneo than the Sulu Sea, and it may be that the differences we observe in underthrust Dangerous Grounds crust are a manifestation of this. Furthermore, Greenfield et al., (2022) note that the lithosphere is thinner in the southwest of Sabah, again suggesting that different processes may have influenced this area compared to those further north.

Overlying the low-velocity layer in Cross-section A is a high velocity layer, also dipping to the south east, with velocities exceeding 4 km/s in our model in what is interpreted as the upper- to mid-crust. High velocities overlying the lower velocities are also observed by Fone et al., (2024). The velocities we observe are consistent with this being mafic to ultramafic material, although, as noted above, the velocities in our models should primarily be interpreted relatively due to the high weight of receiver function observations in the inversion. However, as this high velocity layer appears to lie beneath areas of peridotic rocks near Ranau and ophiolitic rocks near Telupid, we interpret the layer as obducted ophiolitic material. It is not possible to constrain the timing of the emplacement from this study, e.g., it may be the result of late Mesozoic rifting (Tsikouras et al., 2021), or it could have been emplaced earlier (e.g., Cullen and Burton-Johnson 2021).

The crustal structure of the northern tip of Sabah (to the north of SBF2) is distinct from areas to the south, as is particularly seen in Cross-section C (Figure 3(c)), suggesting that distinct geological processes have shaped this region. As similar structure is seen by Fone et al., (2024), this gives us confidence that this is real structure, given that two independent, but complementary, methods have obtained similar results. The change in the character of the crustal structure is in the same place where there is a change in strike of the surface geology, from ~SW-NE to the south to ~WNW-ESE in the north (Tongkul 1990), in the vicinity of Mt Kinabalu. Moreover, it is approximately coincident with where the fast velocity anomaly in the upper mantle that Pilia et al. (2023a) associate with the proto-South China Sea slab terminates. Tongkul (1994) suggests, based on the relationships between sedimentary rocks in this region, that the basement here - Mesozoic oceanic crust - is uplifted relative to the area to the south. Tongkul (1994) further suggests that this region was affected by the collision with the Reed Bank, resulting in N-S compression, while further south the collision was with the Dangerous Grounds block. Gozzard et al., (2018) observe that the crust beneath the Reed Bank has not been thinned in the same way as the Dangerous Grounds block. Franke et al., (2008) also note the presence of the Kudat block off the eastern shore of northernmost Sabah, which active source seismic data suggests has a different crustal structure. It may be that the different properties of blocks colliding with Sabah, as well as the orientation of the collisions, resulted in the contrasting crustal structure we observe today: underthrust material to the south but not at the northern tip of Sabah.

In the east of Sabah, the lower crust and upper mantle beneath stations in the Semporna Peninsula (SBA8 and SBA9) is relatively slow (~3.8-4 km/s for the uppermost mantle compared to 4.3-4.5 km/s elsewhere). This is similar to the results from the two-plane wave tomography of Greenfield et al. (2022). Volcanism in this area occurred until at least 0.2 Ma (Lai et al., 2021) and potentially as recently as 24-27 ka (Kirk, 1968; Bellwood, 1988; cited in Tjia et al., 1992) with hot springs found in the vicinity of Tawau today, with water temperatures of up to 75°C (Siong et al., 1991). Pilia et al. (2023b) and Greenfield et al. (2022) propose that part of the lithosphere has been removed beneath the Semporna Penisula and has been replaced by hot asthenospheric material. This would mean that the remaining crust and mantle would be expected to be warm and thus seismically slow, as we observe here.

Conclusion

We present a high-resolution crustal shear velocity model of Sabah, northern Borneo, from the joint inversion of P receiver functions and surface wave data. We image, for the first, time dipping Dangerous Grounds crust underthrust beneath most of the Crocker Range. This has had the effect of thickening the crust beneath the present-day mountain range, with crustal thicknesses exceeding 40 km. However, beneath Mt Kinabalu, crustal thicknesses are only in the range 30-35km, supporting earlier ideas (Cottam et al., 2013, Sapin et al., 2013, Tsikouras et al., 2021, Pilia et al., 2023b) that some degree of crustal thinning may have been involved in its emplacement. Thinner crust (~25 km) between the Crocker Range and the Circular Basins may be due to extension related to the rollback of the Celebes Sea slab (Hall, 2013), although the amount of extension remains unclear given that pre-extensional crustal thickness remains unknown. Thicker crust (>40 km) beneath the Maliau and other circular basins suggests that these areas have experienced some degree of crustal thickening, which given the late-mid Miocene age of the sediments that have been deformed is likely to have occurred later than the ~21 Ma Sabah Orogeny. Relatively slow velocities in the lower crust and upper mantle beneath the Semporna Peninsula support work by Pilia et al. (2023b) and Greenfield et al. (2021) that lithospheric delamination has occurred here.

Overall, we observe a high degree of heterogeneity in the crustal structure beneath Sabah, on length scales of 10s of kilometres. This highlights the complexity of subduction, collisional, post-subduction, and extensional processes that have shaped Sabah over the Cenozoic, and reinforces the importance of dense instrumentation in order to better understand tectonic activity that has occurred in similar settings.

Global Research Collaboration Statement

Thanks to all those who were involved in the deployment, servicing and recovery of the nBOSS network between March 2018 and January 2020. Many thanks to the landowners throughout Sabah who hosted seismometers on their property. We thank MetMalaysia for providing access to their restricted continuous waveform data recorded by their permanent MY network in Sabah. Fieldwork was conducted under a Research Pass from the Economic Planning Unit (EPU) of the Malaysian Government for the project "North Borneo Uncovered: Orogenic Processes at a Post-Subduction Continental Margin."

Acknowledgements

Seismometers used in the nBOSS network were provided by the University of Cambridge, the University of Aberdeen (Aberdeen University Geophysical Equipment Repository – AUGER), and the Natural Environment Research Council (NERC) Geophysical Equipment Facility though SeisUK (loan 1038). A.G was supported by a Royal Astronomical Society Independent Research Fellowship. S. P was supported by the Natural Environmental Research Council (NERC) Grant NE/R013500/1 and from the European Union's Horizon 2020 Research and Innovation Program under Marie Skłodowska-Curie Grant Agreement 790203. T.G. was supported by an Early Career Fellowship from the Leverhulme Trust. We have made use of several open source Python packages in our analysis and visualisation, including Matplotlib (Hunter, 2007); and ObsPy (Beyreuther et al., 2010). A number of figures were produced using the Generic Mapping Tools version 6 (Wessel et al., 2019). We thank Robert Herrmann for making the Computer Programs in Seismology freely available.

Data availability

The nBOSS dataset is accessible through the EarthScope Data Management Center (https://www.fdsn.org/networks/detail/YC_2018/). Data from the Malaysian national seismic network (https://www.fdsn.org/networks/detail/MY/) are restricted but may be obtained by contacting the Malaysian Meteorological Department. The exceptions to this are stations KKM and LDM which are also available through the Earthscope Data Management Center. The Open Science Framework site for this project, which includes figures for each station analysed, and SAC files for the receiver functions used can be found at: https://osf.io/2zvcg/

Author contributions

A.G.: Formal analysis, conceptualisation, funding acquisition, investigation, resources, visualisation, writing – original draft; **D.C.:** Investigation, resources, writing - review and editing; **N.R.:** Conceptualisation, funding acquisition, resources, investigation, writing – review and editing; **F.T.:** Conceptualisation, resources, investigation; **S.P.:** Investigation, writing – review and editing, funding acquisition; **T.G.:** Investigation, writing – review and editing; **C.B.:** Data curation, investigation.

References

Amaru, M. L. (2007). *Global travel time tomography with 3-D reference models* (Vol. 274). Utrecht University.

Ammon, C. J., Randall, G. E., & Zandt, G. (1990). On the nonuniqueness of receiver function inversions. *Journal of Geophysical Research: Solid Earth*, *95*(B10), 15303-15318.

Bacon, C. A. (2021). *Seismic anisotropy and microseismicity: from crustal formation to subduction termination,* University of Cambridge (United Kingdom)

Bacon, C. A., Rawlinson, N., Pilia, S., Gilligan, A., Wehner, D., Cornwell, D. G., & Tongkul, F. (2022). The Signature of Lithospheric Anisotropy at Post-Subduction Continental Margins: New Insight From XKS Splitting Analysis in Northern Borneo. *Geochemistry, Geophysics, Geosystems*, *23*(11), e2022GC010564.

Balaguru, A., & Nichols, G. (2004). Tertiary stratigraphy and basin evolution, southern Sabah (Malaysian Borneo). *Journal of Asian Earth Sciences*, *23*(4), 537-554.

Barckhausen, U., Engels, M., Franke, D., Ladage, S., & Pubellier, M. (2014). Evolution of the South China Sea: Revised ages for breakup and seafloor spreading. *Marine and Petroleum Geology*, *58*, 599-611.

Bellwood, P. S. (1988). Archaelogical research in south-eastern Sabah. Sabah Museum and State Archives

Beyreuther, M., Barsch, R., Krischer, L., Megies, T., Behr, Y., & Wassermann, J. (2010). ObsPy: A Python toolbox for seismology. *Seismological Research Letters*, *81*(3), 530-533.

Bird, P. (2003). An updated digital model of plate boundaries. *Geochemistry, Geophysics, Geosystems*, *4*(3).

Burton-Johnson, A., Macpherson, C. G., Muraszko, J. R., Harrison, R. J., & Jordan, T. A. (2019). Tectonic strain recorded by magnetic fabrics (AMS) in plutons, including Mt Kinabalu, Borneo: A tool to explore past tectonic regimes and syn-magmatic deformation. *Journal of Structural Geology*, *119*, 50-60.

Burton-Johnson, A., Macpherson, C. G., Millar, I. L., Whitehouse, M. J., Ottley, C. J., & Nowell, G. M. (2020). A Triassic to Jurassic arc in north Borneo: Geochronology, geochemistry, and genesis of the Segama Valley Felsic Intrusions and the Sabah ophiolite. *Gondwana Research*, *84*, 229-244.

Burton-Johnson, A., & Cullen, A. B. (2023). Continental rifting in the South China Sea through extension and high heat flow: An extended history. *Gondwana Research*, 120, 235-263

Cottam, M. A., Hall, R., Sperber, C., Kohn, B. P., Forster, M. A., & Batt, G. E. (2013). Neogene rock uplift and erosion in northern Borneo: evidence from the Kinabalu granite, Mount Kinabalu. *Journal of the Geological Society*, *170*(5), 805-816.

Cullen, A., & Burton-Johnson, A. (2021). [Comment] New zircon radiometric U-Pb ages and Lu-Hf isotopic data from the ultramafic-mafic sequences of Ranau and Telupid (Sabah, eastern Malaysia): Time to reconsider the geological evolution of Southeast Asia?. *Geology*, *49*(11), 541-541.

Forsyth, D., & Uyeda, S. (1975). On the relative importance of the driving forces of plate motion. *Geophysical Journal International*, *43*(1), 163-200.

Franke, D., Barckhausen, U., Heyde, I., Tingay, M., & Ramli, N. (2008). Seismic images of a collision zone offshore NW Sabah/Borneo. *Marine and Petroleum Geology*, *25*(7), 606-624.

Ekström, G. (2011). A global model of Love and Rayleigh surface wave dispersion and anisotropy, 25-250 s. *Geophysical Journal International*, *187*(3), 1668-1686.

Foley, S., Tiepolo, M., & Vannucci, R. (2002). Growth of early continental crust controlled by melting of amphibolite in subduction zones. *Nature*, *417*(6891), 837-840.

Fone, J. W., Rawlinson, N., Pilia, S., Gilligan, A., Cornwell, D., & Tongkul, F. (2024). Ambient noise tomography of northern Borneo reveals evidence of subduction and post-subduction processes. *Journal of Geophysical Research: Solid Earth*, 129, e2024JB029092. https://doi.org/10.1029/2024JB029092

Franke, D. (2013). Rifting, lithosphere breakup and volcanism: Comparison of magma-poor and volcanic rifted margins. *Marine and Petroleum geology*, *43*, 63-87.

Gilligan, A., Roecker, S. W., Priestley, K. F., & Nunn, C. (2014). Shear velocity model for the Kyrgyz Tien Shan from joint inversion of receiver function and surface wave data. *Geophysical Journal International*, *199*(1), 480-498.

Gozzard, S., Kusznir, N., Franke, D., Cullen, A., Reemst, P., & Henstra, G. (2019). South China Sea crustal thickness and oceanic lithosphere distribution from satellite gravity inversion. *Petroleum Geoscience*, *25*(1), 112-128.

Greenfield, T., Gilligan, A., Pilia, S., Cornwell, D. G., Tongkul, F., Widiyantoro, S., & Rawlinson, N. (2022). Post-Subduction Tectonics of Sabah, Northern Borneo, Inferred From Surface Wave Tomography. *Geophysical Research Letters*, *49*(3), e2021GL096117.

Hall, R. (2013). Contraction and extension in northern Borneo driven by subduction rollback. *Journal of Asian Earth Sciences*, *76*, 399-411.

Hall, R., & Spakman, W. (2015). Mantle structure and tectonic history of SE Asia. *Tectonophysics*, *658*, 14-45.

He, K., Zhang, X., Ren, S., & Sun, J. (2016). Deep residual learning for image recognition. In *Proceedings of the IEEE conference on computer vision and pattern recognition* (pp. 770-778).

Herrmann, R. B. (2013). Computer programs in seismology: An evolving tool for instruction and research. *Seismological Research Letters*, *84*(6), 1081-1088.

Hunter, J. D. (2007). Matplotlib: A 2D graphics environment. *Computing in science & engineering*, *9*(03), 90-95.

Hutchison, C. S., Bergman, S. C., Swauger, D. A., & Graves, J. E. (2000). A Miocene collisional belt in north Borneo: uplift mechanism and isostatic adjustment quantified by thermochronology. *Journal of the Geological Society*, *157*(4), 783-793.

Holt, R. A. (1998). *The gravity field of Sundaland-acquisition, assessment and interpretation*. University of London, University College London (United Kingdom)

Huang, Z., Gradstein, F.M., and Louden, K.E., (1991). Subsidence and sedimentation analysis of marginal basins: Celebes Sea and Sulu Sea, Leg 124, Sites 767 and 768, in Silver, E.A., Rangin, C., von Braymann, M.T., et al, Proceedings of the Ocean Drilling Program, *Scientific Results* , 124, 399-407

Johnston, F. K., Turchyn, A. V., & Edmonds, M. (2011). Decarbonation efficiency in subduction zones: Implications for warm Cretaceous climates. *Earth and Planetary Science Letters*, *303*(1-2), 143-152.

Kennett, B. L., Engdahl, E. R., & Buland, R. (1995). Constraints on seismic velocities in the Earth from traveltimes. *Geophysical Journal International*, *122*(1), 108-124.

Kirk, H. J. C. (1968). The igneous rocks of the Sarawak and Sabah. *Geological Survey Borneo Region, Malaysia, Bull*, *5*, 201.

Lai, C. K., Xia, X. P., Hall, R., Meffre, S., Tsikouras, B., Rosana Balangue-Tarriela, M. I., ... & Norazme, N. A. (2021). Cenozoic Evolution of the Sulu Sea Arc-Basin System: An Overview. *Tectonics*, *40*(2), e2020TC006630.

Latiff, A. H. A., & Othman, F. (2020). Earth crustal analysis of Northwest Sabah region inferred from receiver function method. *Warta Geologi*, *46*(2), 59-68.

Levander, A., Schmandt, B., Miller, M. S., Liu, K., Karlstrom, K. E., Crow, R. S., Lee, C.-T. A., & Humphreys, E. D. (2011). Continuing Colorado plateau uplift by delamination-style convective lithospheric downwelling. *Nature*, *472*(7344), 461-465.

Li, C. F., Xu, X., Lin, J., Sun, Z., Zhu, J., Yao, Y., ... & Zhang, G. L. (2014). Ages and magnetic structures of the South China Sea constrained by deep tow magnetic surveys and IODP Expedition 349. *Geochemistry, Geophysics, Geosystems*, *15*(12), 4958-4983.

Li, Z. H., Liu, M., & Gerya, T. (2016). Lithosphere delamination in continental collisional orogens: A systematic numerical study. *Journal of Geophysical Research: Solid Earth*, *121*(7), 5186-5211.

Ligorría, J. P., & Ammon, C. J. (1999). Iterative deconvolution and receiver-function estimation. *Bulletin of the seismological Society of America*, *89*(5), 1395-1400.

Linang, H. T., Pilia, S., Rawlinson, N., Bacon, C. A., Gilligan, A., Cornwell, D. G., & Tongkul, F. (2022). Collision-induced subduction polarity reversal explains the crustal structure of northern Borneo: New results from Virtual Deep Seismic Sounding (VDSS). *Geophysical Research Letters*, *49*(19), e2022GL099123.

Lipke, K. (2008). Seismologic investigation of the Sunda arc region with receiver functions. *Potsdam: University of Potsdam*.

Macpherson, C. G., Chiang, K. K., Hall, R., Nowell, G. M., Castillo, P. R., & Thirlwall, M. F. (2010). Plio-Pleistocene intra-plate magmatism from the southern Sulu Arc, Semporna peninsula, Sabah, Borneo: Implications for high-Nb basalt in subduction zones. *Journal of Volcanology and Geothermal Research*, *190*(1-2), 25-38.

Meju, M. A., Saleh, A. S., Karpiah, A. B., Das, P. S., Miller, R. V., Kho, J. H. W., Alleyne, B.G.T., Rice-Oxley, E.D. & Legrand, X. (2024). Upper mantle flow and crustal deformation patterns beneath the Dangerous Grounds and Borneo where multiple plates converge in South China Sea revealed by 3-D anisotropic magnetotelluric imaging. *Geophysical Journal International*, *239*(3), 1879-1899.

Milsom, J., Holt, R., Hutchison, C. S., Bergman, S. C., Swauger, D. A., & Graves, J. E. (2001). Discussion of a Miocene collisional belt in north Borneo: uplift mechanism and isostatic adjustment quantified by thermochronology: Journal, Vol. 157, 2000, 783–793. *Journal of the Geological Society*, *158*(2), 396-400.

Morley, C. K., & Back, S. (2008). Estimating hinterland exhumation from late orogenic basin volume, NW Borneo. *Journal of the Geological Society*, *165*(1), 353-366.

Pilia, S., Rawlinson, N., Gilligan, A., & Tongkul, F. (2019). Deciphering the fate of plunging tectonic plates in Borneo. *Eos, Transactions American Geophysical Union*, *100*(10), 18-23.

Pilia, S., Rawlinson, N., Hall, R., Cornwell, D. G., Gilligan, A., & Tongkul, F. (2023a). Seismic signature of subduction termination from teleseismic P-and S-wave arrival-time tomography: The case of northern Borneo. *Gondwana Research*, *115*, 57-70.

Pilia, S., Davies, D. R., Hall, R., Bacon, C. A., Gilligan, A., Greenfield, T., Tongkul, F., Kramer, S. C., Wilson, C. R., Ghelichkhan, S., Cornwell, D. G., Colli, L., & Rawlinson, N. (2023b). Post-subduction tectonics induced by extension from a lithospheric drip. *Nature Geoscience*, 1-7.Rangin, C., Spakman, W., Pubellier, M., & Bijwaard, H. (1999). Tomographic and geological constraints on subduction along the eastern Sundaland continental margin (South-East Asia). *Bulletin de la Société géologique de France*, *170*(6), 775-788.

Rawlinson, N. (2018). *Northern Borneo Orogeny Seismic Survey* [Data set]. International Federation of Digital Seismograph Networks. https://doi.org/10.7914/SN/YC_2018

Roberts, G. G., White, N., Hoggard, M. J., Ball, P. W., & Meenan, C. (2018). A Neogene history of mantle convective support beneath Borneo. *Earth and Planetary Science Letters*, *496*, 142-158.

Sapin, F., Hermawan, I., Pubellier, M., Vigny, C., & Ringenbach, J. C. (2013). The recent convergence on the NW Borneo Wedge—a crustal-scale gravity gliding evidenced from GPS. *Geophysical Journal International*, *193*(2), 549-556.

Schaeffer, A. J., & Lebedev, S. (2013). Global shear speed structure of the upper mantle and transition zone. *Geophysical Journal International*, *194*(1), 417-449.

Siong, L. P., Intang, F., & On, C. F. (1991). Geothermal prospecting in the Semporna Peninsula with emphasis on the Tawau area. *Geological Society of Malaysia, Bulletin 29*, 135-155

Syuhada, S., Pranata, B., Anggono, T., Ramdhan, M., Zulfakriza, Z., Febriani, F., Prasetio, A.D., Dewi, C.N., Hasib, M., & Sulaiman, A. (2022). Crustal velocity structure in Borneo Island using receiver function inversion. *Acta Geophysica*, *70*(6), 2529-2553.

Takashima I., Nazri, A. A., Lim, P. S., Koseki, T., Mouri, Y., Nasution, A., & Sucipta, I. E., (2004). Thermoluminescence age determination of quaternary volcanic rocks and alteration products at Tawau area, Sabah, Malaysia. *Journal of the Geothermal Research Society of Japan*, *26*(3), 273-283.

Tang, Q., & Zheng, C. (2013). Crust and upper mantle structure and its tectonic implications in the South China Sea and adjacent regions. *Journal of Asian Earth Sciences*, *62*, 510-525.
Tjia, H. D., Komoo, I., Ali, C. A., & Tahir, S. H. (1992). Geology of Taman Bukit Tawau, Semporna Peninsula, Sabah. *Geological Society of Malaysia, Bulletin 31*, 113-131

Tian, Z., Gao, Y., Wang, P., & Tang, H. (2024). Formation and Tectonic Evolution of Ophiolites in the Sabah Area (Borneo, SE Asia). *Minerals*, *14*(11), 1078.

Tongkul, F. (1990). Structural style and tectonics of Western and Northern Sabah. *Geological Society of Malaysia, Bulletin 27*, 227-239

Tongkul, F. (1991). Tectonic evolution of Sabah, Malaysia. *Journal of Southeast Asian Earth Sciences*, *6*(3-4), 395-405.

Tongkul, F. (1994). The geology of Northern Sabah, Malaysia: its relationship to the opening of the South China Sea Basin. *Tectonophysics*, *235*(1-2), 131-147.

Tongkul, F., and Chang, F. K. (2003) Structural geology of the Neogene Maliau Basin, Sabah. *Geological Society of Malaysia, Bulletin 47*, 51-61

Tsikouras, B., Lai, C. K., Ifandi, E., Teo, C. H., & Xia, X. P. (2021). New zircon radiometric U-Pb ages and Lu-Hf isotopic data from the ultramafic-mafic sequences of Ranau and Telupid (Sabah, eastern Malaysia): Time to reconsider the geological evolution of Southeast Asia?. *Geology*, *49*(7), 789-793.

Wehner, D., Blom, N., Rawlinson, N., Böhm, C., Miller, M. S., Supendi, P., & Widiyantoro, S. (2022). SASSY21: A 3-D Seismic Structural Model of the Lithosphere and Underlying Mantle Beneath Southeast Asia From Multi-Scale Adjoint Waveform Tomography. *Journal of Geophysical Research: Solid Earth*, *127*(3), e2021JB022930.

Wessel, P., Luis, J. F., Uieda, L., Scharroo, R., Wobbe, F., Smith, W. H., & Tian, D. (2019). The generic mapping tools version 6. *Geochemistry, Geophysics, Geosystems*, *20*(11), 5556-5564.

Zandt, G., Gilbert, H., Owens, T. J., Ducea, M., Saleeby, J., & Jones, C. H. (2004). Active foundering of a continental arc root beneath the southern Sierra Nevada in California. *Nature*, *431*(7004), 41-46.

Zenonos, A., De Siena, L., Widiyantoro, S., & Rawlinson, N. (2019). P and S wave travel time tomography of the SE Asia-Australia collision zone. *Physics of the Earth and Planetary Interiors*, *293*, 106267.

Figures

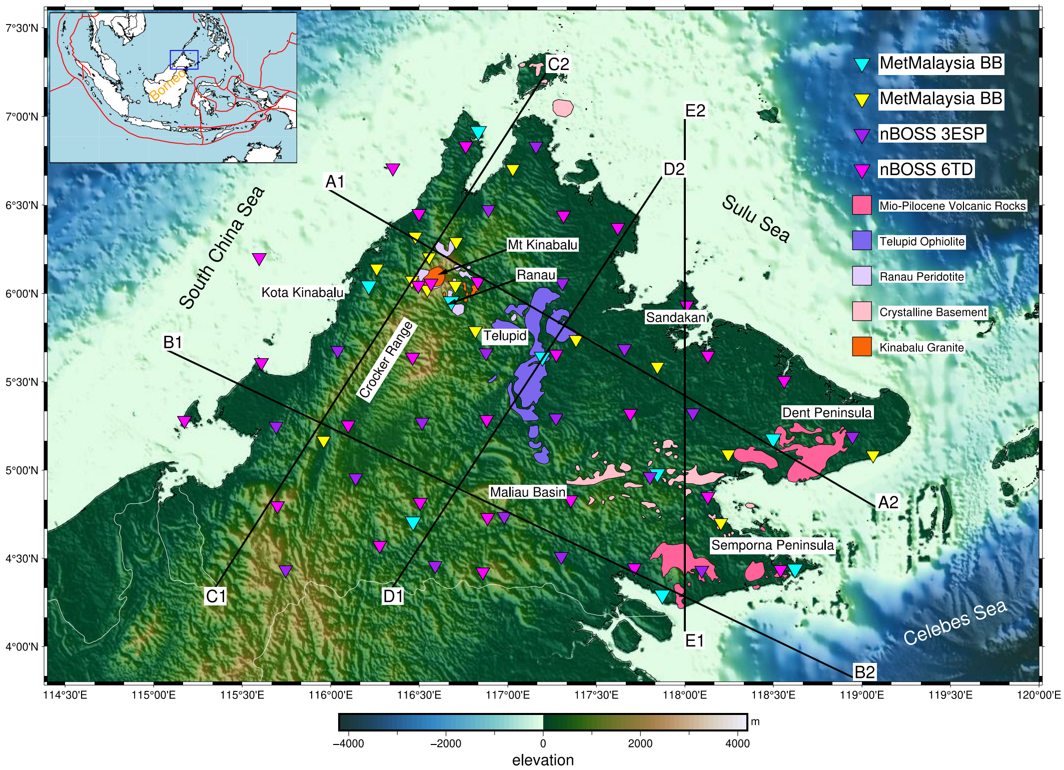

Figure 1: Map of seismometer stations in Sabah used in this study. Blue triangles are MetMalaysia seismometers deployed before 2017, yellow triangles are MetMalaysia seismometers deployed after 2017. Pink (6TD) and Purple (3ESP) triangles are seismometers deployed as part of the nBOSS project. Lines of section are shown: A1-A2 (6.56°N 115.97°E 4.78°N 119.09°E), B1-B2 (5.691°N 115.05°E - 3.82°N 118.96°E), C1-C2 (4.25°N 115.30°E - 7.26°N 117.23°E), D1-D2(4.25°N 116.30°E - 6.67°N 117.88°E) E1-E2 (4°N 118°E - 7°N 118°E). Geological units are plotted after Hall (2013). The inset map shows the wider geographical area, with the area of the main map highlighted by the blue box, and plate boundaries after Bird (2003), are shown by red lines.

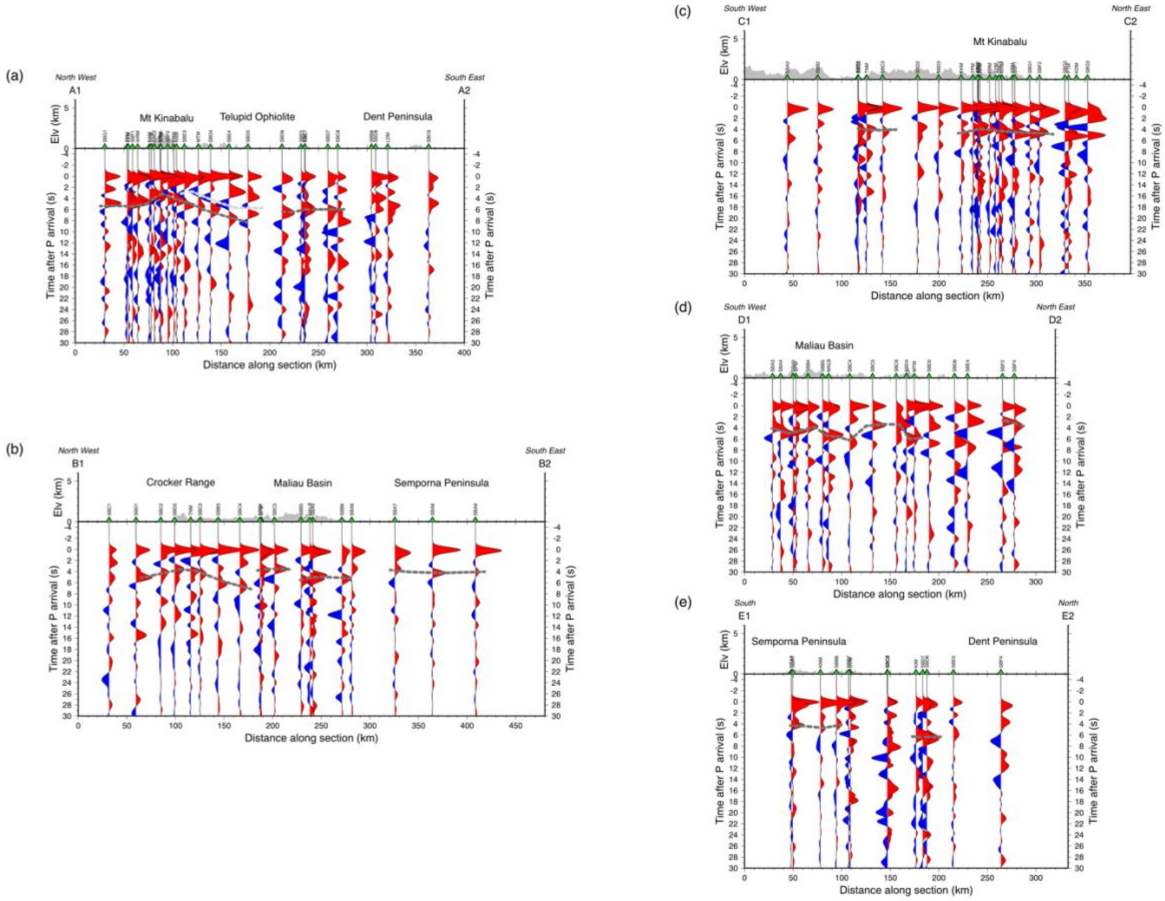

Figure 2: Stacked receiver functions along the lines (a) A1-A2, (b) B1-B2, (c) C1-C2, (d) D1-D2, and (e) E1-E2. Positive arrivals are filled red, and negative arrivals are filled blue. In both cases receiver functions from stations within 50 km of each line have been projected onto the section, along with their respective station (green triangles), and topography is plotted above. The dark grey dashed line highlights positive arrivals, likely from the P-to-S conversion at the Moho. The light grey dashed line highlights negative arrivals corresponding to a velocity increase with depth in the crust.

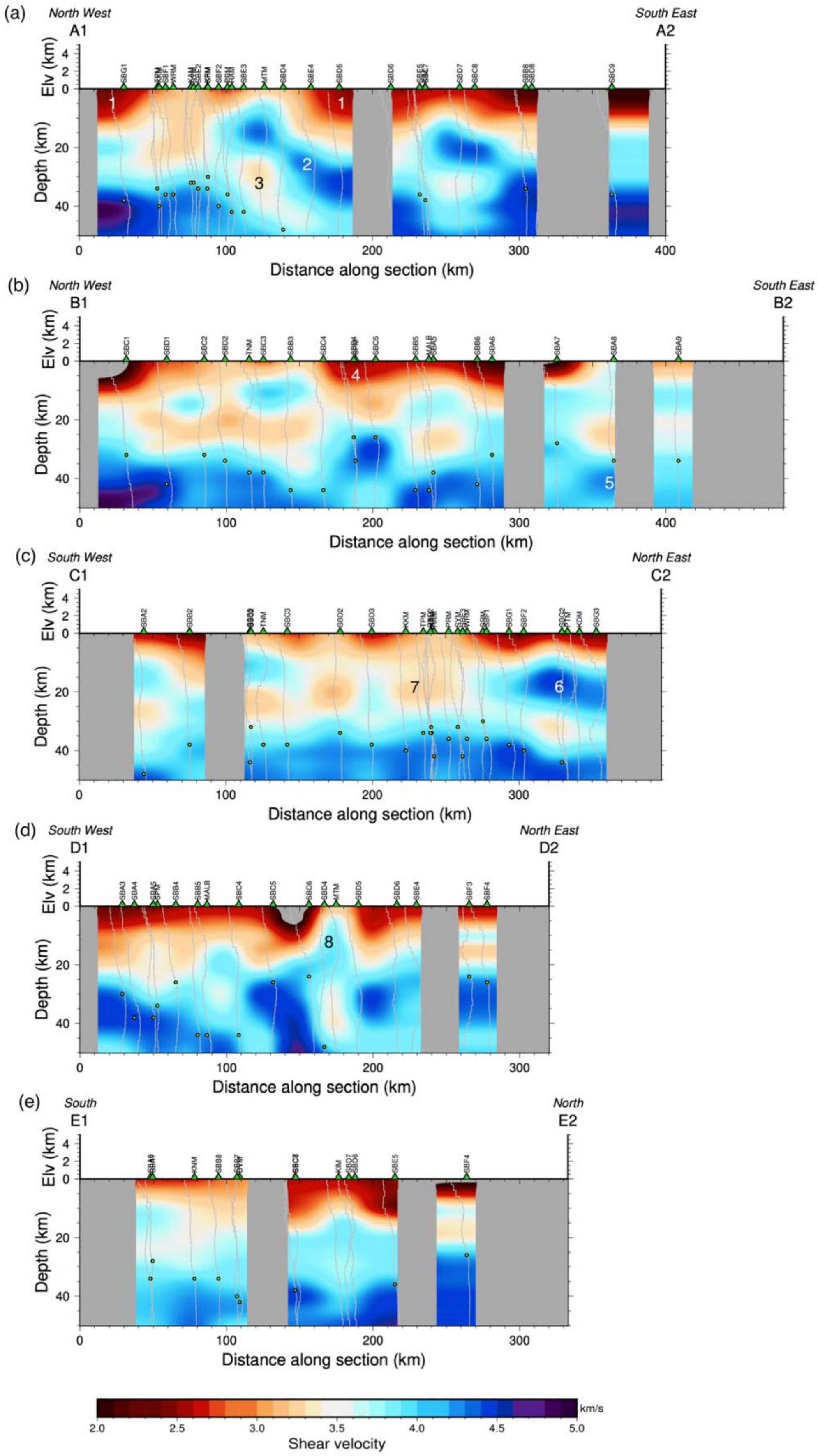
(a) North West South East
A1 A2
(b) North West South East
B1 B2
(c) South West North East
C1 C2
(d) South West North East
D1 D2
(e) South North
E1 E2
Elv (km)
Depth (km)
Distance along section (km)
km/s
Shear velocity

1141

Figure 3: Shear velocity vs depth along lines (a) A1-A2, (b) B1-B2, (c) C1-C2, (d) D1-D2, (e) E1-E2 from the joint inversion of receiver function and surface wave data. 1-D models from stations within 50 km of the line of section are interpolated to make the cross-sections. Grey areas indicate areas with no station coverage. Green triangles mark the location of stations. Topography along the line of section is plotted above. Labelled velocity anomalies 1-8 are discussed in the text.

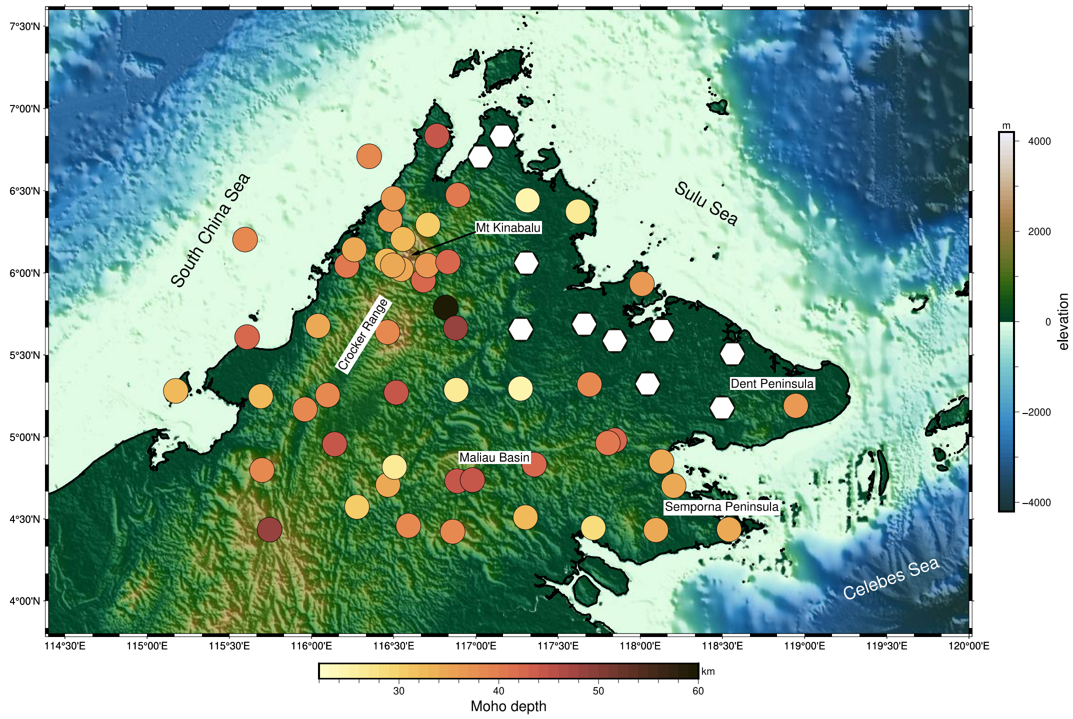

Figure 4: Moho depths at seismometer stations in Sabah picked from 1D shear velocity models from the joint inversion of receiver function and surface wave data. The colour of the circle indicated Moho depth for the station located at that point, as shown in the scale. White hexagons are locations where there was no clear Moho to be picked or where there were multiple plausible velocity discontinuities that could be the Moho.

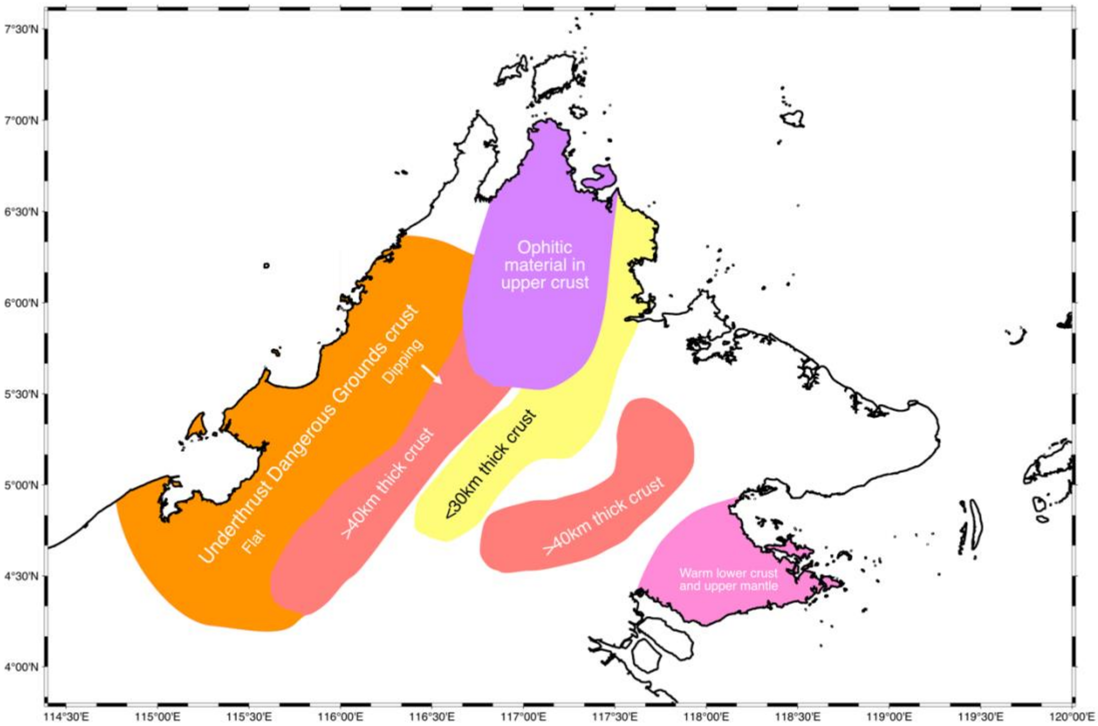

Figure 5: Summary map highlighting the key interpretations from this study from the shear velocity models derived from the joint inversion of receiver function and surface wave data.

Imaging subduction, collision, and extension in northern Borneo: Constraints from receiver functions

Amy Gilligan(1),* David G. Cornwell(1), Nicholas Rawllinson(2), Felix Tongkul(3), Simone Pilia(4), Tim Greenfield(2), Conor Bacon(5)

1. *School of Geosciences, University of Aberdeen, Aberdeen, UK*
2. *Department of Earth Sciences, University of Cambridge, Cambridge, UK*
3. *Faculty of Science and Natural Resources, Universiti Malaysia Sabah, Kota Kinabalu, Malaysia*
4. *College of Petroleum Engineering and Geosciences, King Fahd University of Petroleum and Minerals, Dhahran, Saudi Arabia*
5. *Lamont-Doherty Earth Observatory, Columbia University, Palisades, New York, USA*

** Corresponding author: amy.gilligan@abdn.ac.uk*

Supplementary Material

Supplementary table 1: The name, instrument type, and location of the seismometers used in this study, together with the number of good receiver functions after quality control, and the crustal thickness estimated from the joint inversion of receiver function and surface wave data. Where the crustal thickness is N/A this is because there were no good receiver functions for that station. Where crustal thickness is 'X' these are stations where it was not possible to estimate the crustal thickness from the velocity model.

Network	Station	Instrument type	Latitude (N)	Longitude (E)	# of receiver functions	Crustal thickness (km)
YC	SBA2	3ESP	4.43506	115.74560	76	48
YC	SBA3	6TD	4.57347	116.27660	74	30
YC	SBA4	3ESP	4.45879	116.58977	73	38
YC	SBA5	6TD	4.42271	116.85881	84	38
YC	SBA6	3ESP	4.51025	117.30176	18	32
YC	SBA7	6TD	4.44587	117.71442	47	28
YC	SBA8	3ESP	4.43208	118.09522	183	34

YC	SBA9	6TD	4.43637	118.53992	76	34
YC	SBB2	6TD	4.79788	115.69913	62	38
YC	SBB3	3ESP	4.95640	116.14096	126	44
YC	SBB4	6TD	4.81717	116.50497	36	26
YC	SBB5	6TD	4.73101	116.88574	82	44
YC	MALB	3ESP	4.73740	116.97997	51	44
YC	SBB6	6TD	4.83194	117.35575	54	42
YC	SBB7	3ESP	4.96355	117.80282	70	40
YC	SBB8	6TD	4.85014	118.12941	79	34
YC	SBC1	6TD	5.28108	115.17476	24	32
YC	SBC2	3ESP	5.24880	115.69165	114	32
YC	SBC3	6TD	5.25540	116.09856	48	38
YC	SBC4	3ESP	5.27107	116.51573	76	44
YC	SBC5	6TD	5.28637	116.88076	73	26
YC	SBC6	3ESP	5.29518	117.27165	19	24
YC	SBC7	6TD	5.32075	117.69134	23	42
YC	SBC8	3ESP	5.32373	118.04523	13	X
YC	SBC9	3ESP	5.19098	118.94610	54	36
YC	SBD1	6TD	5.60898	115.60830	42	42
YC	SBD2	3ESP	5.67735	116.03960	55	34
YC	SBD3	6TD	5.63900	116.46225	89	38
YC	SBD4	3ESP	5.66416	116.87691	86	48
YC	SBD5	6TD	5.65637	117.27355	28	X
YC	SBD6	3ESP	5.68750	117.65900	28	X
YC	SBD7	6TD	5.64967	118.12955	80	X
YC	SBD8	6TD	5.50699	118.56041	34	X

YC	SBE1	6TD	6.20282	115.5963	33	38
YC	SBE2	6TD	6.04611	116.49462	83	34
YC	KINA	6TD	6.05826	116.56593	0	N/A
YC	SBE3	6TD	6.06708	116.83097	63	42
YC	SBE4	3ESP	6.05975	117.30715	48	X
YC	SBE5	6TD	5.93328	118.01012	37	36
YC	SBF1	6TD	6.45216	116.49845	48	36
YC	SBF2	3ESP	6.47376	116.89069	42	40
YC	SBF3	6TD	6.44177	117.31431	95	24
YC	SBF4	6TD	6.37312	117.62083	30	26
YC	SBG1	6TD	6.70950	116.35092	22	38
YC	SBG2	6TD	6.83352	116.76262	49	44
YC	SBG3	3ESP	6.83170	117.15904	55	X
MY	DVM	STS-2.5	4.98038	117.84421	11	42
MY	FSM	STS-2.5	5.0855	119.0627	0	N/A
MY	KAM	STS-2.5	6.0745	116.4583	45	32
MY	KDM	SS-1 Ranger	6.9167	116.8333	0	N/A
MY	KIM	STS-2.5	5.587083	117.844717	48	X
MY	KKM	STS-2	6.0443	116.2147	61	40
MY	KNM	STS-2.5	4.7026	118.203	82	34
MY	KPM	STS-2.5	6.0227	116.545417	21	34
MY	LDM	STS-2.5	5.1777	118.498	35	X
MY	MTM	STS-2.5	5.789333	116.81665	37	60
MY	PRM	STS-2.5	6.0455	116.70375	51	36
MY	PTM	STS-2.5	6.70523	117.0283	39	X

MY	RAM	STS-2.5	5.9546	116.681	64	42
MY	SDM	SS-1 Ranger	5.6409	117.195	0	N/A
MY	SGM	STS-2.5	5.0912	118.2446	0	N/A
MY	SMM	SS1-Ranger	4.439838	118.622028	0	N/A
MY	SPM	STS-2	4.7083	116.465	9	34
MY	SRM	STS-2.5	6.29265	116.708383	36	30
MY	SYM	STS-2.5	6.20585	116.5559	42	32
MY	TLM	STS-2.5	5.7391	117.385	0	N/A
MY	TNM	STS-2.5	5.168633	115.960183	27	38
MY	TPM	STS-2.5	6.1427	116.2596	19	34
MY	TSM	SS-1 Ranger	4.2936	117.8725	0	N/A
MY	WRM	STS-2.5	6.3229	116.47825	29	36

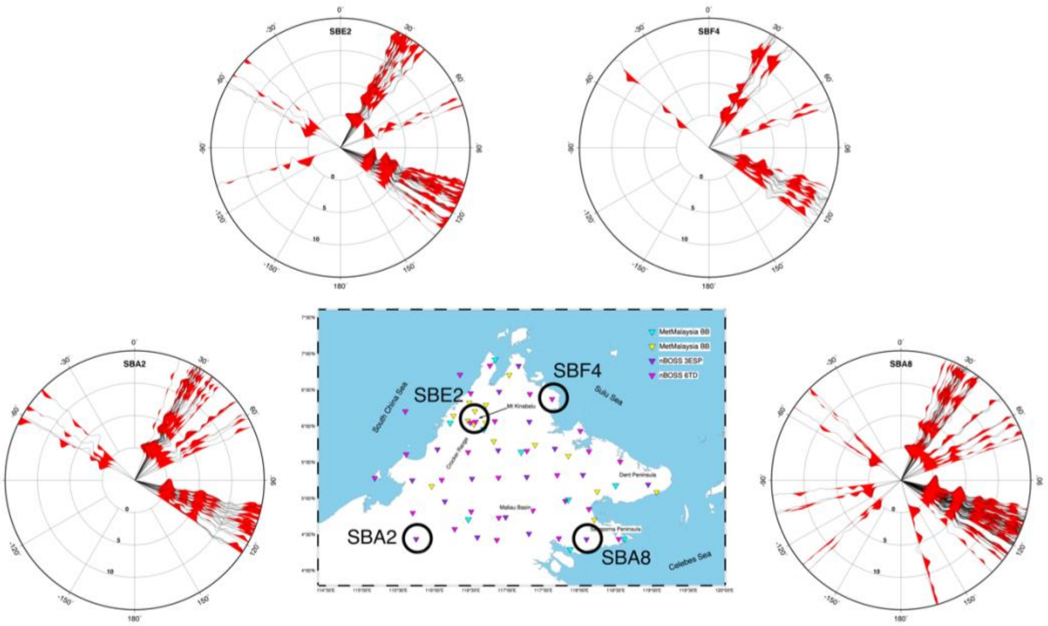

Supplementary figure 1: Examples of the receiver functions of individual events used in the station stacks for four stations across Sabah: SBA2, SBE2, SBF4, and SBA9, and a map indicating the station locations. Receiver functions are plotted with respect to backazimuth with positive amplitudes filled red.

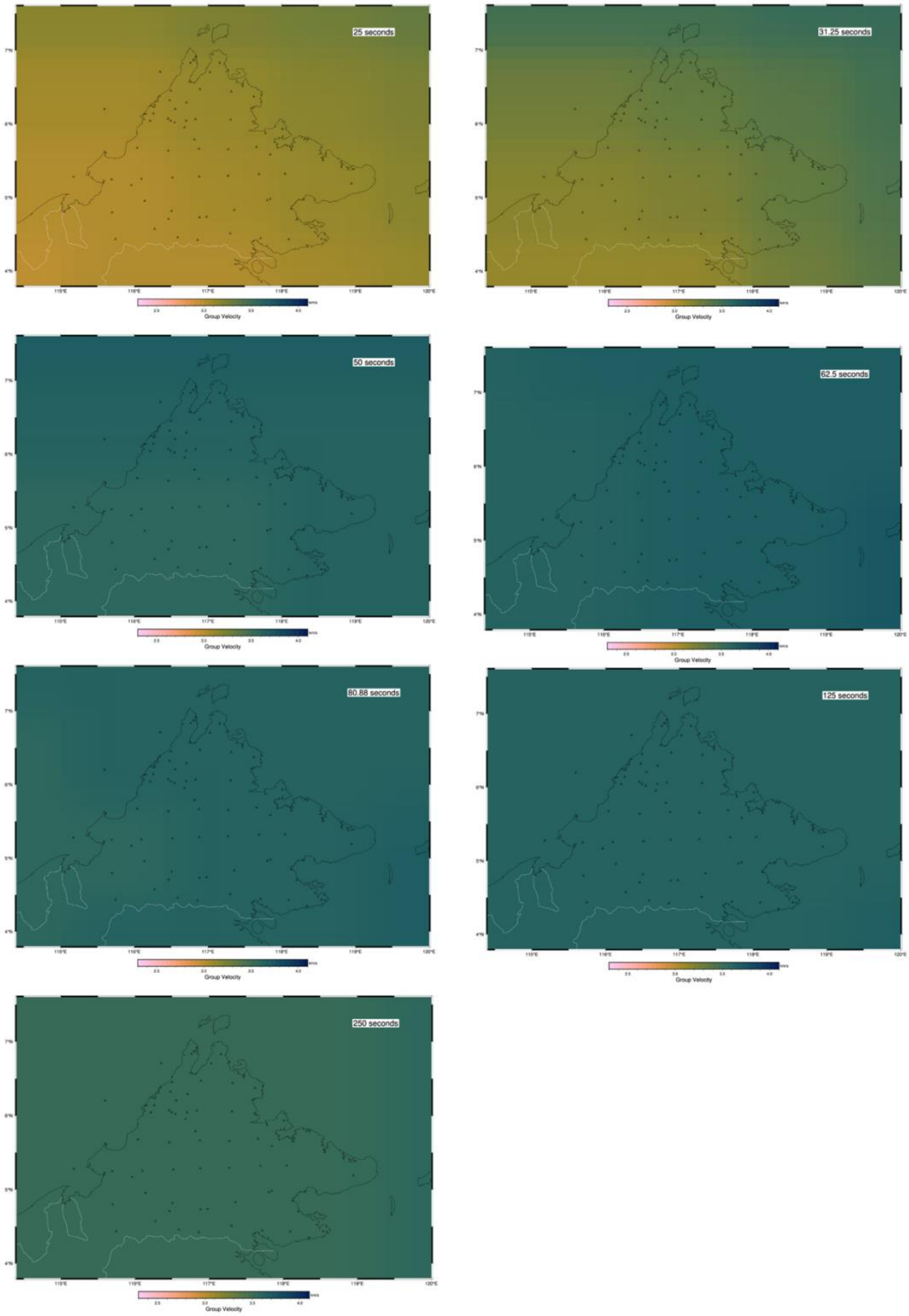

Supplementary figure 2: Group velocity maps for the GDM52 model (Ekstrom, 2011), for the periods 25s, 31.25s, 50s, 62.5s, 80.88s, 125s, and 250s.

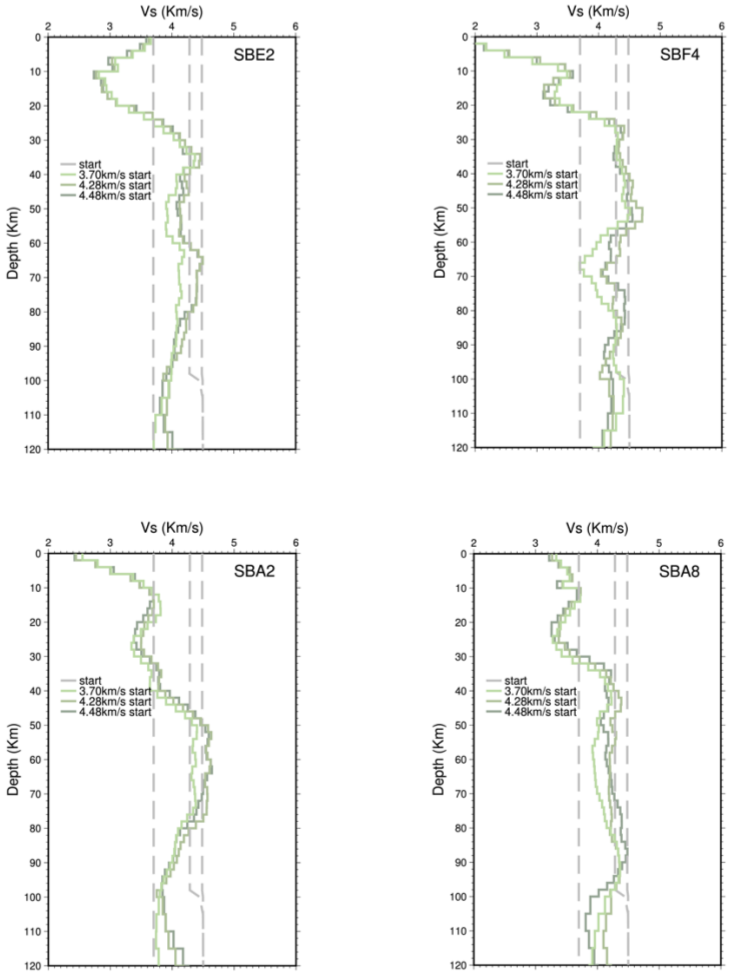

Supplementary figure 3: Examples of models of shear velocity vs depth from the joint inversion of surface wave and receiver function data four stations SBA2, SBE2, SBF4, and SBA8 with a p value of 0.1. On each shear velocity model the coloured lines show the different models that result from testing different starting models: 4.48 km/s, 4.28 km/s, and 3.70 km/s.

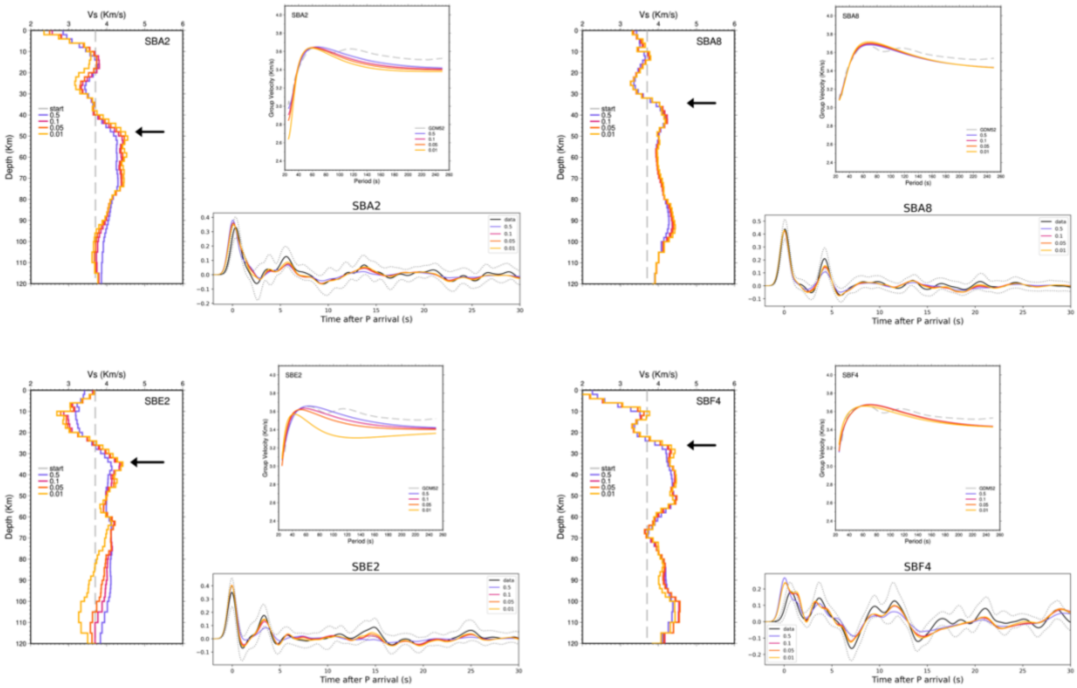

Supplementary figure 4: Examples of models of shear velocity vs depth from the joint inversion of surface wave and receiver function data, and the receiver functions for these models for four stations across Sabah: SBA2, SBE2, SBF4, and SBA9On each of the shear velocity and receiver function plots the coloured lines show the results from testing different weights of receiver function and surface wave data. On the shear velocity plots, the black arrow indicates the depth that is picked for the Moho in each example. On the receiver function plots, the receiver function data are shown in black.

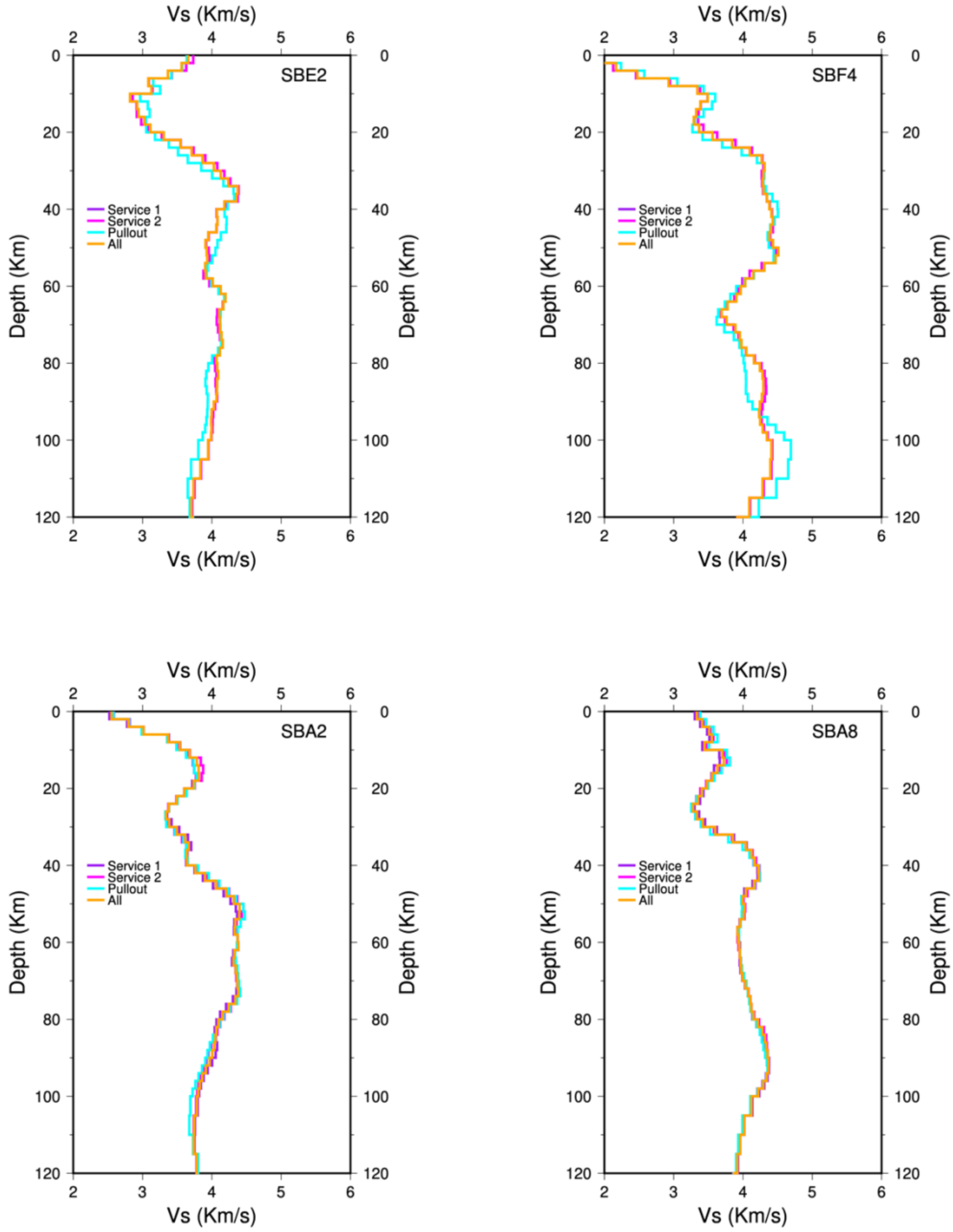

Supplementary figure 5: Examples of models of shear velocity vs depth from the joint inversion of surface wave and receiver function data four stations SBA2, SBE2, SBF4, and SBA8 with a p value of 0.1. On each shear velocity model the coloured lines show the different models that result from testing different subsets of the receiver function data: Service 1 (purple) is from the inversion of stacked receiver functions for events between March 2018-Sept 2018, Service 2 (magenta) is from the inversion of stacked receiver functions from events between Sept 2018-March 2019, Pullout is from the inversion of stacked receiver functions from events between March 2019-Jan 2020, and All is from the inversion of stacked receiver functions for the whole time period, as shown in Supplementary figure 1. For each station, the same surface wave dispersion data was used for each of the inversions.

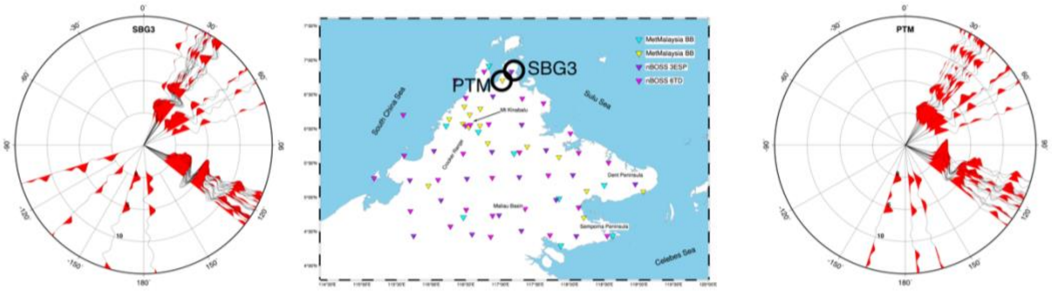

Supplementary figure 6: Examples of the receiver functions of individual events used in the station stacks for SBG3 (left) and PTM (right) and a map indicating the station locations. Receiver functions are plotted with respect to backazimuth with positive amplitudes filled red.

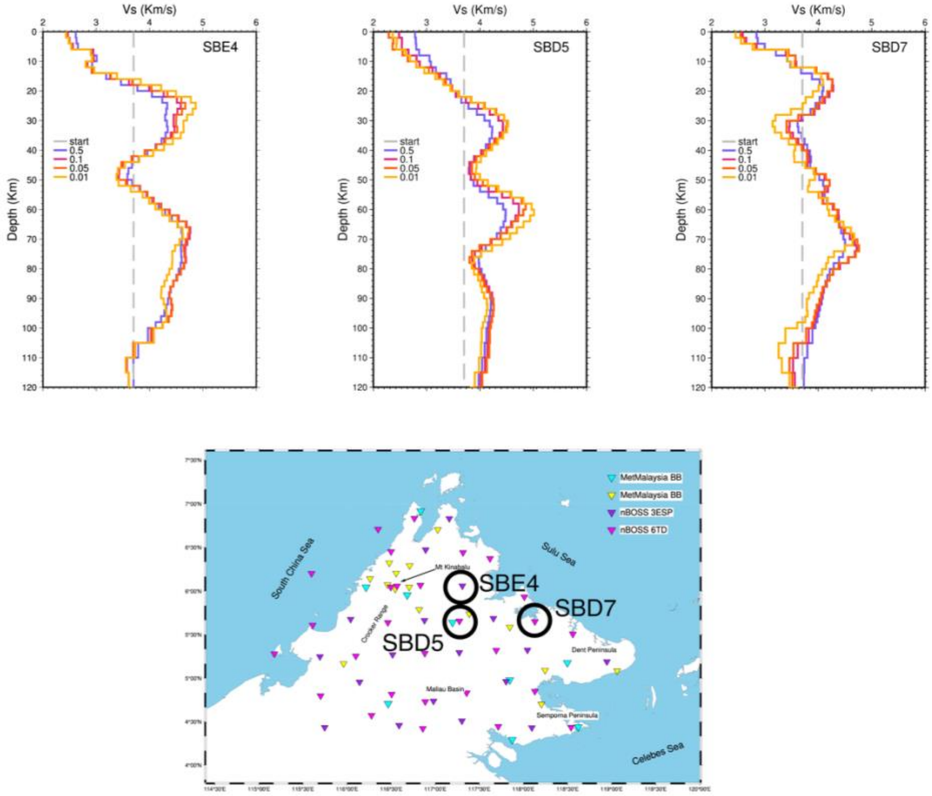

Supplementary figure 7: Examples of models of shear velocity vs depth from the joint inversion of surface wave and receiver function data for stations where a Moho was challenging to identify in this study. SBE4 and SBD5 are examples of stations with two potential discontinuities, while SBD7 shows a gradual increase in velocities over a wide depth range. On each shear velocity model the coloured lines show the different models that result from testing different weights of receiver function and surface wave data.

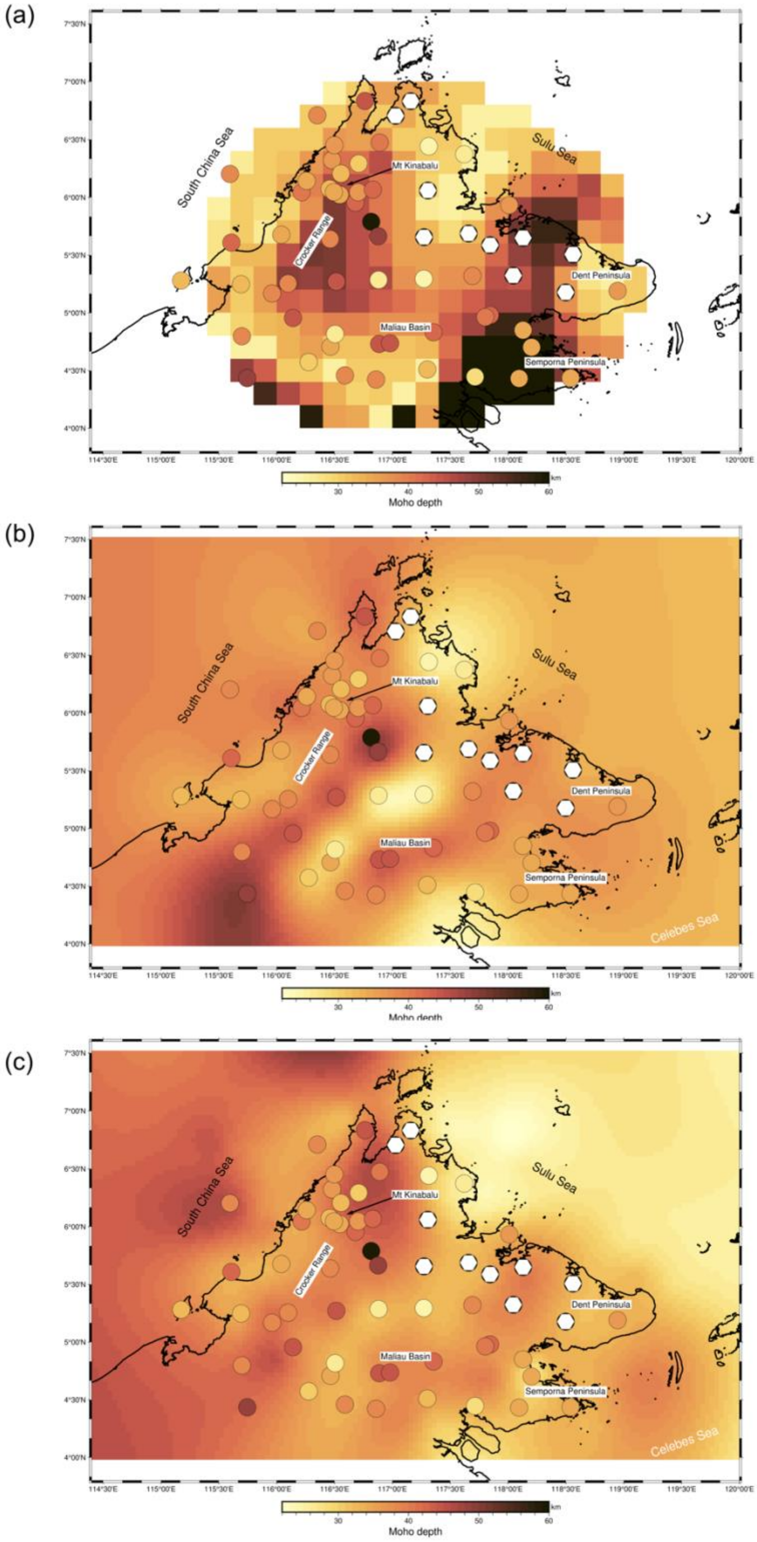

Supplementary figure 8: Comparison of Moho depths from this study (circles) with other Moho depth estimates from other studies of the region. (a) comparison with the Moho depth from Greenfield et al., (2022) based on the 4.1km/s velocity contour in their shear velocity model, (b) comparison with the Moho depth from Linang et al, (2022) from the interpolation of crustal depths obtained from stacked VDSS traces, assuming the depths reflect the Moho beneath stations, (c) comparison with the Moho depth from Linang et al,

(2022) from the interpolation of crustal depths at reflection points in the VDSS method.